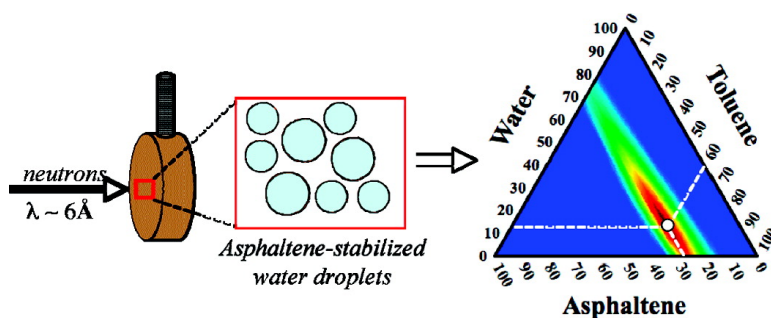


Water-in-Model Oil Emulsions Studied by Small-Angle Neutron Scattering: Interfacial Film Thickness and Composition

Vincent J. Verruto, and Peter K. Kilpatrick

Langmuir, 2008, 24 (22), 12807-12822 • DOI: 10.1021/la802095m • Publication Date (Web): 24 October 2008

Downloaded from <http://pubs.acs.org> on December 9, 2008



More About This Article

Additional resources and features associated with this article are available within the HTML version:

- Supporting Information
- Access to high resolution figures
- Links to articles and content related to this article
- Copyright permission to reproduce figures and/or text from this article

[View the Full Text HTML](#)

Water-in-Model Oil Emulsions Studied by Small-Angle Neutron Scattering: Interfacial Film Thickness and Composition

Vincent J. Verruto[†] and Peter K. Kilpatrick^{*‡}

Department of Chemical & Biomolecular Engineering, North Carolina State University, Raleigh, North Carolina 27695, and Department of Chemical & Biomolecular Engineering, University of Notre Dame, Notre Dame, Indiana 46556

Received July 3, 2008. Revised Manuscript Received September 3, 2008

The ever-increasing worldwide demand for energy has led to the upgrading of heavy crude oil and asphaltene-rich feedstocks becoming viable refining options for the petroleum industry. Traditional problems associated with these feedstocks, particularly stable water-in-petroleum emulsions, are drawing increasing attention. Despite considerable research on the interfacial assembly of asphaltenes, resins, and naphthenic acids, much about the resulting interfacial films is not well understood. Here, we describe the use of small-angle neutron scattering (SANS) to elucidate interfacial film properties from model emulsion systems. Modeling the SANS data with both a polydisperse core/shell form factor as well as a thin sheet approximation, we have deduced the film thickness and the asphaltenic composition within the stabilizing interfacial films of water-in-model oil emulsions prepared in toluene, decalin, and 1-methylnaphthalene. Film thicknesses were found to be 100–110 Å with little deviation among the three solvents. By contrast, asphaltene composition in the film varied significantly, with decalin leading to the most asphaltene-rich films (30% by volume of the film), while emulsions made in toluene and methylnaphthalene resulted in lower asphaltenic contents (12–15%). Through centrifugation and dilatational rheology, we found that trends of decreasing water resolution (i.e., increasing emulsion stability) and increasing long-time dilatational elasticity corresponded with increasing asphaltene composition in the film. In addition to the asphaltenic composition of the films, here we also deduce the film solvent and water content. Our analyses indicate that 1:1 (O/W) emulsions prepared with 3% (w/w) asphaltenes in toluene and 1 wt % NaCl aqueous solutions at pH 7 and pH 10 resulted in 80–90 Å thick films, interfacial areas around 2600–3100 cm²/mL, and films that were roughly 25% (v/v) asphaltenic, 60–70% toluene, and 8–12% water. The increased asphaltene and water film composition at pH 10 versus pH 7, along with unique dynamic interfacial tension profiles, suggested that the protonation state of carboxylic moieties within asphaltenes impacts the final film properties. This was further supported when we characterized similar asphaltenic emulsions that also contained 9-anthracene carboxylic acid (ACA). Addition of this aromatic acid led to slightly thinner films (70–80 Å) that were characteristically more aqueous (up to 20% by volume) and 5–6% (v/v) ACA. This unique *in situ* characterization (deduced entirely from SANS data from emulsion samples) of the entire film composition calls for further investigation regarding the role this film-based water plays in emulsion stability.

Introduction

With the current market prices for crude oil around all-time highs,¹ heavy crude oils continue to be a more attractive and profitable feedstock option for many processing applications. However, heavy crude oils are well-known for the formation of stable water-in-oil emulsions that contribute to pipeline deposits, corrosion, catalyst poisoning, and transporting difficulties.^{2–10} Heavy crudes with low API gravity are rich in naturally surface-active species, including naphthenates, resins, and asphaltenes, the *n*-heptane-insoluble/toluene-soluble fraction of crude oil. Asphaltenes attract particular attention for their ability to form

elastic films that sheath water droplets and prevent coalescence. Thus, evaluating emulsion stability has been a consistent focus of many studies, including resistance to coalescence under heating,^{11,12} centrifugation,^{13,14} microwave-induced destabilization,^{11,15} or an electric field.^{16–22} Recent investigations have focused on measurable mechanical properties of the films by interfacial tensiometry^{23–25} and rheological techniques.^{26–32} A key criticism of these latter experiments is the length scale

* To whom correspondence should be addressed. E-mail: peter.kilpatrick@nd.edu.

[†] North Carolina State University.

[‡] University of Notre Dame.

(1) Donnelly, J. J. *Pet. Technol.* **2007**, *59*, 128–138.

(2) Blair, C. *Chem. Ind.* **1960**, 538 Interfacial Films Affecting the Stability of Petroleum Emulsions.

(3) Berridge, S.; Thew, M.; Loriston, A. *J. Inst. Pet.* **1968**, *54*, 333.

(4) Thompson, D. G.; Taylor, A. S.; Graham, D. E. *Colloids Surf.* **1985**, *15*, 175–189.

(5) Clark, P. E.; Pilehvari, A. *J. Pet. Sci. Eng.* **1993**, *9*, 165–181.

(6) Sanchez, L. E.; Zakin, J. L. *Ind. Eng. Chem. Res.* **1994**, *33*, 3256–3261.

(7) Aomari, N.; Gaudu, R.; Cabioc'h, F.; Omari, A. *Colloids Surf., A* **1998**, *139*, 13–20.

(8) Fingas, M.; Fieldhouse, B. *Mar. Pollut. Bull.* **2003**, *47*, 369.

(9) Langevin, D.; Poteau, S.; Henaut, I.; Argillier, J. F. *Oil Gas Sci. Technol.* **2004**, *59*, 511–521.

(10) Farah, M. A.; Oliveira, R. C.; Caldas, J. N.; Rajagopal, K. J. *Pet. Sci. Eng.* **2005**, *48*, 169–184.

(11) Xia, L.; Lu, S.; Cao, G. *J. Colloid Interface Sci.* **2004**, *271*, 504–506.

(12) Gafonova, O.; Yarranton, H. J. *Colloid Interface Sci.* **2001**, *241*, 469.

(13) McLean, J. D.; Kilpatrick, P. K. *J. Colloid Interface Sci.* **1997**, *189*, 242.

(14) McLean, J. D.; Kilpatrick, P. K. *J. Colloid Interface Sci.* **1997**, *196*, 23.

(15) Fortuny, M.; Oliveira, C.; Melo, R.; Nele, M.; Coutinho, R.; Santos, A. *Energy Fuels* **2007**, *21*, 1358–1364.

(16) Chen, T.; Mohammed, R.; Bailey, A.; Luckham, P.; Taylor, S. *Colloids Surf., A* **1994**, *83*, 273–284.

(17) Fordedal, H.; Sjöblom, J. *J. Colloid Interface Sci.* **1996**, *181*, 589–594.

(18) Sjöblom, J.; Aske, N.; Auflem, I. H.; Brandal, O.; Havre, T. E.; Saether, O.; Westvik, A.; Johnsen, E. E.; Kallevik, H. *Adv. Colloid Interface Sci.* **2003**, *100–102*, 399–473.

(19) Aske, N.; Kallevik, H.; Sjöblom, J. *J. Pet. Sci. Eng.* **2002**, *36*, 1–17.

(20) Beetge, J. H.; Horne, B. O. *SPE Int. Symp. Oilfield Chem., 2004* **2004**, (21) Hemmingsen, P. V.; Silset, A.; Hannisdal, A.; Sjöblom, J. *J. Dispersion Sci. Technol.* **2005**, *26*, 615–627.

(22) Sullivan, A. P.; Zaki, N. N.; Sjöblom, J.; Kilpatrick, P. K. *Can. J. Chem. Eng.* **2007**, *85*.

(23) Ese, M. H.; Yang, X.; Sjöblom, J. *Colloid Polym. Sci.* **1998**, *276*, 800.

(24) Zhang, L. Y.; Breen, P.; Xu, Z.; Masliyah, J. H. *Energy Fuels* **2007**, *21*, 274–285.

(25) Zhang, L. Y.; Lopetinsky, R.; Xu, Z.; Masliyah, J. H. *Energy Fuels* **2005**, *19*, 1330–1336.

(26) Dodd, C. G. *J. Phys. Chem.* **1960**, *64*, 544.

discrepancy between the experimental O/W interface and that of real-life emulsions (with particular implications on the diffusion, adsorption, and coalescence time scales during emulsion aging) and the difficulty in resolving that discrepancy. The use of micropipets to create micrometer scale droplets and test their interfacial properties is an example of an elegant solution to this issue.^{33–35} However, despite the expanding knowledge base regarding asphaltenic film properties, the current literature is limited regarding the measurement of some critical aspects of these emulsion-stabilizing films: the film thickness and its composition. So while film thickness and asphaltene interfacial concentration have been measured in experiments using Langmuir–Blodgett^{36,37} and the thin-liquid film techniques,^{38,39} neither technique examines an actual emulsion interface. Alternatively, we will demonstrate in this work the ability to characterize *in situ* water-in-model oil emulsions using small-angle neutron scattering (SANS), extracting key particulars on both the average film thickness and composition, and in the process shed light on the role of solvent, aqueous phase pH, and even organic additives in dictating these physical and chemical properties of the films.

Throughout the literature, SANS has been used to characterize nanoscale structures, including self-assembled asphaltenic aggregates, for which the literature continues to expand.^{40–56} Structural information such as size and shape are valuable when relating the properties of interfacial assemblies to those in the

bulk phase. Also, the degree of solvent entrainment within asphaltenic aggregates and the composition of the entrained solvent have been reported using SANS.^{53,56} This kind of composition information for asphaltenic aggregates is unique to SANS, further demonstrating its value in petroleum research.

For emulsion-forming systems, SANS offers the ability to probe droplets in their native geometric conformation. This differs from other popular techniques which do not necessarily mimic realistic interfacial geometry conditions. One example is neutron reflectometry, which employs a single planar oil/water interface of fairly large total area (several mm²), at which an adsorbed asphaltene film may possess very different structural and chemical properties from that of an emulsion, in which asphaltenes adsorb upon micrometer-sized droplets, with individual surface areas often between 10–100 μm². In fact, SANS has already been applied to emulsion and emulsion-like systems with documented characterization ability. Whether it was vesicles^{57,58} or liposomes,^{58–60} intrabilayer polymerization,⁶¹ or surfactant-stabilized emulsions,^{62–64} researchers have demonstrated the strength of SANS as a characterization tool for interfacial self-assembly.

Furthermore, in a recent study by Jestin et al., the authors performed SANS on emulsions made with dilute asphaltene solutions (0.3 wt %) in xylene and at various pH conditions.⁶⁵ In their work, three different asphaltene fractions, recovered from the same crude by precipitation with pentane, heptanes, or octane, were used to prepare the emulsions. With increasing precipitant carbon chain length, the authors observed an increase in emulsion film thickness (113–149 Å), accompanied by a decrease in the calculated asphaltene composition within the films (17–11% v/v). The modest changes in film thickness and asphaltene concentration with increasing pH were attributed to the ionization of acidic asphaltene subfractions due to deprotonation at basic pH.

The study described here shares many similarities with the work of Jestin et al.,⁶⁵ but it is unique in many important ways. Similarly, both investigations make use of SANS to evaluate the properties of the physical properties of the emulsion, including the surface area-to-volume ratio (*S/V*) and the interfacial film thickness (Δ). Also in both studies, the asphaltenic composition of the interfacial film is extracted from experimental data. However, in the aforementioned study, the authors evaluated the interfacial asphaltene concentration (in mg/m²) by projecting the change in bulk asphaltene concentration after emulsification (determined by UV–visible spectrophotometry) onto the total droplet surface area (from *S/V*). In this study, we demonstrate that the asphaltene film concentration can be recovered from SANS data without the need for such before-and-after bulk phase comparisons. Additionally, we evaluate the composition of the film, with respect to its asphaltene volume fraction, and, in the latter part of the investigation, the solvent and water film content as well, whereas the authors of the former study assumed that the film was composed only of asphaltene and solvent. We are able to do this by our application of a polydisperse core/shell

- (27) Spiecker, P. M.; Kilpatrick, P. K. *Langmuir* **2004**, *20*, 4022–4032.
 (28) Bouriat, P.; El Kerri, N.; Graciaa, A.; Lachaise, J. *Langmuir* **2004**, *20*, 7459.
 (29) Dicharry, C.; Arla, D.; Sinquin, A.; Graciaa, A.; Bouriat, P. *J. Colloid Interface Sci.* **2006**, *297*, 785–791.
 (30) Yarranton, H. W.; Sztukowski, D. M.; Urrutia, P. *J. Colloid Interface Sci.* **2007**, *310*, 246–252.
 (31) Yarranton, H. W.; Urrutia, P.; Sztukowski, D. M. *J. Colloid Interface Sci.* **2007**, *310*, 253–259.
 (32) Yang, X.; Verruto, V. J.; Kilpatrick, P. K. *Energy Fuels* **2007**, *21*, 1343–1349.
 (33) Yeung, A.; Dabros, T.; Czarnecki, J.; Masliyah, J. *Proc. R. Soc. London, Ser. A* **1999**, *455*, 3709.
 (34) Moran, K.; Yeung, A.; Czarnecki, J.; Masliyah, J. *Colloids Surf., A* **2000**, *174*, 147–157.
 (35) Tsamantakis, C.; Masliyah, J.; Yeung, A.; Gentzis, T. *J. Colloid Interface Sci.* **2005**, *284*, 176–183.
 (36) Chandra, M. S.; Xu, Z.; Masliyah, J. H. *Energy Fuels* **2008**, *22*, 1784–1791.
 (37) Cadena-Nava, R. D. *Energy Fuels* **2007**, *21*, 2129.
 (38) Khristov, K.; Taylor, S.; Czarnecki, J.; Masliyah, J. *Colloids Surf., A* **2000**, *174*, 183–196.
 (39) Panchev, N.; Khristov, K.; Czarnecki, J.; Exerowa, D.; Bhattacharjee, S.; Mashyah, J. *Colloids Surf., A* **2008**, *315*, 74–78.
 (40) Sheu, E. Y.; Storm, D. A.; De Tar, M. J. *Non-Cryst. Solids* **1991**, *131–133*, 341–347.
 (41) Sheu, E. Y.; Liang, K. S.; Sinha, S. K.; Overfield, R. E. *J. Colloid Interface Sci.* **1992**, *153*, 399–410.
 (42) Liu, Y. C.; Sheu, E. Y.; Chen, S. H.; Storm, D. A. *Fuel* **1995**, *74*, 1352.
 (43) Thiyagarajan, P.; Hunt, J. E.; Winans, R. E.; Anderson, K. B.; Miller, J. T. *Energy Fuels* **1995**, *9*, 829.
 (44) Fenistein, D.; Barre, L.; Broseta, D.; Espinat, D.; Livet, A.; Roux, J. N.; Scarsella, M. *Langmuir* **1998**, *14*, 1013.
 (45) Miller, J. T.; Fisher, R. B.; Thiyagarajan, P.; Winans, R. E.; Hunt, J. E. *Energy Fuels* **1998**, *12*, 1290–1298.
 (46) Roux, J. N.; Broseta, D.; Deme, B. *Langmuir* **2001**, *17*, 5085.
 (47) Gawrys, K. L.; Spiecker, P. M.; Kilpatrick, P. K. *Pet. Sci. Technol.* **2003**, *21*, 461–489.
 (48) Mason, T. G.; Lin, M. Y. *Phys. Rev. E* **2003**, *67*.
 (49) Tanaka, R.; Hunt, J.; Winans, R.; Thiyagarajan, P.; Sato, S.; Takanohashi, T. *Energy Fuels* **2003**, *17*, 127.
 (50) Espinat, D.; Fenistein, D.; Barre, L.; Frot, D.; Briolant, Y. *Energy Fuels* **2004**, *18*, 1243–1249.
 (51) Gawrys, K. L.; Kilpatrick, P. K. *J. Colloid Interface Sci.* **2005**, *288*, 325–334.
 (52) Sirota, E. B. *Energy Fuels* **2005**, *19*, 1290–1296.
 (53) Gawrys, K. L.; Blankenship, G. A.; Kilpatrick, P. K. *Langmuir* **2006**, *22*, 4487–4497.
 (54) Gawrys, K. L.; Blankenship, G. A.; Kilpatrick, P. K. *Energy Fuels* **2006**, *20*, 705–714.
 (55) Merdignac, I.; Espinat, D. *Oil Gas Sci. Technol.* **2007**, *62*, 7–32.
 (56) Verruto, V. J.; Kilpatrick, P. K. *Energy Fuels* **2007**, *21*, 1217–1225.

- (57) Gallová, J.; Uhríková, D.; Hanulová, M.; Teixeira, J.; Balgavy, P. *Colloids Surf., B* **2004**, *38*, 11–14.
 (58) Kucerka, N.; Kiselev, M.; Balgavy, P. *Eur. Biophys. J.* **2004**, *33*, 328.
 (59) Nawroth, T.; Conrad, H.; Dose, K. *Phys. B* **1989**, *156*, 477.
 (60) Balgavy, P.; Dubnickova, M.; Kucerka, N.; Kiselev, M.; Yaradaikin, S.; Uhríkova, D. *Biochim. Biophys. Acta* **2001**, *1512*, 40.
 (61) McKelvey, C. A.; Kaler, E. W. *J. Colloid Interface Sci.* **2002**, *245*, 68.
 (62) Reynolds, P. A.; Gilbert, E. P.; White, J. W. *J. Phys. Chem. B* **2000**, *104*, 7012.
 (63) Reynolds, P. A.; Gilbert, E. P.; White, J. W. *J. Phys. Chem. B* **2001**, *105*, 6925.
 (64) Staples, E.; Penfold, J.; Tucker, I. *J. Phys. Chem. B* **2000**, *104*, 606.
 (65) Jestin, J.; Simon, S.; Zupancic, L.; Barre, L. *Langmuir* **2007**, *23*, 10471–10478.

Table 1. Elemental Composition of the HOW Asphaltenes Used in the Investigations Described Within

element	% by weight	
	solvent dependence	pH and ACA addition
C	79.1	79.4
H	8.1	8.3
N	2.0	2.2
S	8.2	8.0
O	2.6	2.1
H/C	1.2	1.2

form factor model (to samples of varying deuterium composition); this modeling was not employed by Jestin et al.,⁶⁵ who estimated the asphaltenic composition in the film simply by dividing the calculated surface concentration by the film thickness determined from SANS. Also, the part pertaining to oil-side chemistry in that study focused on asphaltene chemistry variation with precipitant, which was presumed to be related to the varying concentration of coprecipitated resins, whereas here we investigate the role of the host solvent aromaticity by studying emulsions made in 1-methylnaphthalene, toluene, and decalin. Furthermore, in the section of that study regarding the impact of water-side chemistry (pH) on interfacial properties, the authors focused again solely on the surface packing aspect of the asphaltenes, with no focus on the impact on other film constituents, that is, water, solvent, or dopants, as we investigate here with a polynuclear aromatic acid (9-anthracene carboxylic acid).

Materials and Methods

Sample Preparation. Asphaltenes were recovered from Hondo crude oil, a California offshore crude, in adherence to the techniques described in ASTM D-2295 (IP143). A separate detailed description of this recovery process can be found elsewhere.⁵⁶ We refer to these materials as Hondo whole (HOW) asphaltenes, as they were not further fractionated in any way. Combustion elemental analysis (CHNSO) was performed in duplicate at the University of Alberta on a Carlo Erba EA-1108 elemental analyzer. The average elemental compositions are listed in Table 1.

Solutions for the solvent dependence substudy were prepared by dissolving the appropriate amount of HOW asphaltenes to achieve a concentration of 1% (w/w) in toluene-*d*₈ (CDN, D-40, 99.6% D), 1-methylnaphthalene-*d*₁₀ (CDN, D-1300, 98.9% D), and decalin-*d*₁₈ (CDN, D-885, 98.8% D). To simplify, we will refer to the deuterated and hydrogenated isotopes with a preceding *d*- or *h*-, that is, *d*-toluene represents toluene-*d*₈. A 68:32 *d*:*h*-decalin mixture was necessary to achieve near identical scattering length densities of the decalin and D₂O phases. The methylnaphthalene and decalin solutions were placed in an oven at 40 °C for 6 h to reduce the solvent viscosity and enhance the dissolution kinetics. Upon return to room temperature no precipitation from either solution was observed. All model oils were shaken for 24 h prior to their use in the emulsification protocol described below. Model oils were prepared in pure solvents so as to reduce ambiguity in determining film composition that could arise in mixed solvent systems from selective partitioning of aromatic solvents within self-assembled asphaltenic structures.⁵⁶

Since asphaltenes represent only a portion of the surface-active species in crude oil, we also evaluated film properties when a relevant surface-active species, 9-anthracene carboxylic acid (ACA), was added to asphaltenes. From previous investigations, in which various naphthenic and aromatic organic acids were systematically added into different crude oils, we observed an increase in critical electric field (i.e., emulsion stability). This enhanced stability was thought to result from a synergistic relationship between the asphaltenes and ACA at the interface, in which the ACA molecules acted as a secondary cross-linker. Presumably, with its fused aromatic anthracene ring structure, ACA can participate in physical cross-links with asphaltenes by overlapping π orbitals. The carboxylic acid group, located on the central anthracene ring, gives rise to the

molecule's interfacial activity. Solutions for this part of the study were prepared by dissolving the appropriate mass of HOW asphaltenes to achieve a concentration of 3% (w/w) in *d*-toluene, *h*-toluene (Fisher, T290), 80:20 *d*:*h*-toluene, or 60:40 *d*:*h*-toluene. When samples with added acid were prepared, we added enough 9-anthracene carboxylic acid (ACA) (Aldrich, A8,940-5) or the deuterated version (CDN, D-6063, 98% D) to achieve a concentration of 0.4% (w/w). Alone, ACA was sparingly soluble in toluene (<10 mM), but we have observed enhanced solubility when it was dissolved into crude oils or into solutions containing asphaltenes (indicated by the disappearance of the large visible yellow specks in the vial). However, at this asphaltene concentration of 3 wt %, the maximum ACA/HOW ratio (w/w) we could achieve was 0.133, which equated to the aforementioned 0.4% (w/w). In an effort to assist dissolution of ACA, we sonicated the solutions in a Fisher FS9H sonication bath at 45 °C for 15–30 min.

The aqueous phase for our emulsions was a 1% (w/w) NaCl solution in deionized H₂O (18.2 M Ω ·cm) prepared using a Millipore Milli-Q system, D₂O (CDN, D-175, 99.9% D), 89:11 D₂O/H₂O, or 80:20 D₂O/H₂O. These were pH-adjusted to either 7 or 10 using dilute HCl or DCl and NaOH or NaOD. The organic phase consisted of the previously described asphaltene or asphaltene/ACA solutions. Equal volumes (1.5 mL) of both phases were added to an 8 mL glass vial, in which emulsification was administered at 15 000 rpm, for 5 min each, on a Virtis Cyclone IQ² homogenizer equipped with a 7 mm rotor-stator tip. Due to the density differences between the aqueous and organic phases, and the size of the droplets, the emulsion droplets always settled to 2/3 of the total sample height. Given the prepared water volume fraction of 0.5 in the emulsion, the settled phase was approximately 75% (v/v) water.

As part of the investigation, we employed a rinsing protocol to physically remove asphaltenic aggregates from the bulk phase. A detailed description and schematic of this procedure can be found in the Supporting Information. This procedure ensured that the scattering signal would arise solely from the emulsion droplets and their asphaltenic films and not from free asphaltenic aggregates. Due to their affinity for the interface, and with ample interfacial aging for physical cross-linking to occur, "consolidated" asphaltenes do not appreciably desorb during solvent replacement,²⁷ and emulsion stability is not compromised by such a procedure.²⁴ In the least, the data from rinsed emulsions represent the irreversibly adsorbed interfacial material, from which we believe much of the emulsion stability behavior is derived.

Neutron Scattering. For the solvent dependence study, nonrinsed emulsions were scattered at Argonne National Laboratory (ANL) at the Intense Pulsed Neutron Source (IPNS) using both the small-angle neutron diffractometer (SAND) and small-angle scattering instrument (SASI). Accessible Q ranges were 0.0035–0.6 and 0.007–1.5 \AA^{-1} for SAND and SASI, respectively. All samples were run in quartz cells having a 2 mm path length. As a result of emulsion droplet settling, some samples had to be shaken every 5–15 min to keep the droplets suspended. Scattering times were typically 1–2 h for emulsions, and background solvent blanks were run for 45 min. Transmission for each SAND run was collected over 15 min, while on SASI the transmission was collected simultaneously with scattering. Alternatively, rinsed emulsions pertaining to this investigation were scattered at the National Institute for Standards and Technology (NIST), specifically at the NIST Center for Neutron Research (NCNR) on the NG3 30-m SANS beamline within the Center for High Resolution Neutron Scattering (CHRNS) in Gaithersburg, MD. On NG3, our selected Q window was 0.0029–0.0996 \AA^{-1} .

In the second investigation of the study, in which changes in aqueous phase pH and ACA composition were implemented, ACA-free and ACA-added emulsion samples were scattered on the aforementioned SAND instrument at ANL with the same Q range. Again, samples were scattered for 1–2 h, with an extra 15 min for transmission collection. Emulsions devoid of ACA were also scattered at NIST but on the NG7 30-m SANS beamline using two instrument configurations that spanned a Q range of 0.0025–0.446 \AA^{-1} . Sample scattering times varied depending on the sample contrast and

instrument configuration, but they ranged between 5 and 60 min. Transmission on each sample at NIST was collected using the 13-m configuration, with an attenuated beam, over the duration of 3 min. For samples where the solvent phase contained 40% *h*-toluene, we used 1 mm path length cylindrical quartz cells. For all other samples, 2 mm path length cells were employed.

Neutron Data Reduction. Data collected at NIST were reduced using Igor Pro (Wavemetrics) and macros provided on the NCNR Web site and discussed in further detail by Kline.⁶⁶ These macros subtracted the stray neutron background and scattering of the quartz cell and accounted for the transmission of the sample and cell as well as the detector efficiency. This adjusts the scattering data to an absolute intensity scale, facilitating comparisons among data from different sources. The data collected at ANL was reduced with their Integrated Spectral Analysis Workbench (ISAW) software, using scripts that ultimately normalized the data to an absolute intensity scale much like the NIST Igor Pro macros.

For the nonrinsed samples, we accounted for the contribution of the dispersed and continuous phases to the scattering signal by subtracting from the reduced sample scattering intensity the individual phases weighted by their volume fraction in the emulsion:

$$I_{\text{sub}} = I_{\text{emul}} - \phi_{\text{CO}} I_{\text{POC}} - \phi_{\text{w}} I_{\text{w}} \quad (1)$$

where I_{sub} is the bulk asphaltene- and water-subtracted scattering data, I_{emul} and I_{w} are the respective scattering intensities for the whole emulsion sample and the aqueous phase, I_{POC} is the smoothed continuous phase scattering intensity, and ϕ_{CO} and ϕ_{w} are the volume fractions of the continuous and dispersed phases, respectively. This analysis required the recovery of the residual “creamed oil” phase, which consisted of asphaltenes not used in film formation and thus left behind in the bulk solvent. This was achieved by centrifuging samples at 3500–5000 rpm for 5–60 min on an IEC-Centra CL2 tabletop centrifuge. The discrepancy in centrifugation times is a result of the greater viscosity of 1-methylnaphthalene and its density being nearly equal to that of the aqueous phase. After centrifugation, the supernatant was removed and centrifuged an additional time at 5000 rpm for 5 min and then transferred to a quartz sample cell for scattering.

Rinsed emulsion samples consisted of water droplets with a protective interfacial film, surrounded by fresh asphaltene-free solvent. Depending on the hydrogen content of each phase and the sample composition, the incoherent background varied significantly. The incoherent scattering contribution to the data was removed by preparing a $Q^4 * I$ vs Q^4 plot, fitting a line to data where $Q^4 > 1 \times 10^{-4} \text{ \AA}^{-4}$, and subtracting the value of that slope from the absolute intensity data. This type of background subtraction has been documented elsewhere.⁶¹

Neutron Data Analysis. Reduced emulsion data were analyzed using a combination of special-case scattering approximations and a polydisperse core/shell form factor model (since the spherical water droplets are enveloped by an asphaltenic film). In Figure 1, we illustrate some of the contrast conditions that can be achieved for such geometry, simply by varying the deuterium/hydrogen content of the different phases. By relative contrast of the three components of the system, the core, the shell, and the free external bulk phase, we observe the conditions of complete contrast mismatch (cf. Figure 1a) as well as contrast-matching of the core and bulk (1b), core and shell (1c), and shell and bulk (1d) phases. The observed scattering behavior from each of the four conditions in Figure 1 should be distinct, the degree of which will depend on the scattering length density (SLD) values associated with the black, gray, and white phases as well as the relative size of the shell compared to the core. This SLD contrast is dictated by the isotopic substitution of deuterium (²H or D) for hydrogen (¹H) in the materials that make up each phase. Furthermore, by selectively varying the deuterium composition of these different materials, we can evaluate their impact on the overall scattering behavior and perhaps even ascertain their inclusion,

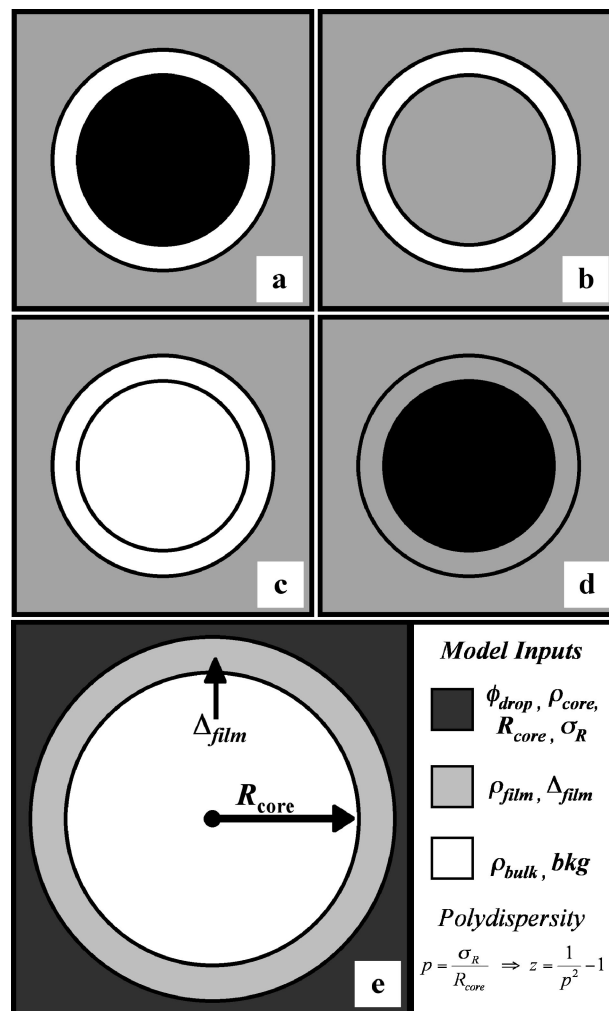


Figure 1. Concept of contrast variation and contrast-matching, applied to a core/shell scattering geometry. Four cases are presented: (a) All three phases have unique SLD values, (b) the core and bulk phases have matching SLD values, (c) the core and shell are matched, and (d) the shell and bulk phases are contrast-matched. The bold lines around each phase are drawn in only to identify geometric boundaries for the reader. (e) Schematic of the core/shell model of Bartlett and Ottewill⁷¹ with characteristic physicochemical inputs.

say, within the interfacial film. For example, contrast variation methods were applied by Reynolds et al. to evaluate properties of micrometer scale water-in-hexadecane emulsions stabilized by polyisobutylene-derived surfactants.⁶² Contrast variation enabled the authors to evaluate the emulsion specific interfacial area ($S/V \sim 0.6\text{--}0.7 \text{ m}^2/\text{mL}$) and total surfactant interfacial concentration ($\Gamma_{\text{ads}} \sim 0.8\text{--}2.2 \text{ mg}/\text{m}^2$). Staples et al. used contrast variation to elucidate the mixed surface compositions for dilute submicrometer hexadecane-in-water emulsions (6.4% by volume) made with mixtures of nonionic (C_{12}E_6) and anionic (SDS) surfactants.⁶⁴ This was accomplished using both hydrogenated and perdeuterated forms of C_{12}E_6 . Unique changes in scattering behavior with increasing total surfactant concentration (2–14 mM) corresponded to decreases in SDS surface composition, deduced from interfacial layer SLD changes. In the work presented here, we use SLD contrast variation to elucidate properties of the entire emulsion system, including the total surface area, interfacial film thickness, and, particularly, the film composition.

In the solvent dependence study, the samples were prepared such that the scattering length density of the aqueous phase would match that of the bulk solvent. At this contrast-matched condition, the scattering should arise solely from the interfacial material (cf. Figure 1b) and, for the nonrinsed emulsions, bulk phase aggregates. Through either the aforementioned physical or mathematical removal of these

aggregates from the scattering system, the resulting curve contains only the interfacial film scattering.

Studies on polymers adsorbed or grafted to silica surfaces provide an approximation of thin shell scattering from core/bulk contrast-matched samples.^{67–69} The approximation is valid if the shell thickness is much smaller than the core radius. The scattering from such samples is modeled as that of a planar thin sheet, and eq 2 can be used to evaluate the film thickness and, to some extent, the film composition:

$$I(Q) = I_0 Q^{-2} \exp(-R_{G,TS}^2 Q^2) + \text{bkg} \quad (2)$$

where I_0 is the limit of $I(Q)$ as Q approaches zero, $R_{G,TS}$ is the radius of gyration of a thin sheet, and bkg is the residual background scattering. The square of the radius of gyration is the second moment of the mass distribution about an object's center of mass, and for a uniform thin sheet the thickness, Δ_{TS} , is related to the radius of gyration by

$$R_{G,TS}^2 = \frac{\Delta_{TS}^2}{12} \quad (3)$$

Thus, using the negative slope from a plot of $\ln[Q^2 I(Q)]$ versus Q^2 , one can calculate the average film thickness. Note that this linearization works only when emulsion droplets appear as hollow spheres; that is, the SLD of the core and bulk materials are identical. For liposome- and vesicle-forming systems, this is straightforward, as the core and bulk phases consist of the same material (typically water), which is one reason this approach has been well-documented for such systems.^{57,58} In emulsion systems, perfect contrast-matching of the aqueous and organic phases is nontrivial and requires great precision.⁶²

In addition, the I_0 term in eq 4 is a function of the amount of adsorbed material in the film, as shown in eq 4 below:

$$I_0 = 2(\Delta\rho)^2 \left(\frac{S}{V} \right) \left(\frac{\Gamma_{\text{ads}}}{\rho_{\text{ads}}} \right)^2 \quad (4)$$

where $(\Delta\rho)^2$ is the SLD contrast term between the *adsorbate* and the matched core/bulk phases, (S/V) is the droplet surface area per unit volume of emulsion sample, Γ_{ads} is the mass concentration of the adsorbate per unit surface area, and ρ_{ads} is the adsorbate bulk density. This makes SANS even more appealing because it removes the need for a comparative analysis of the bulk concentration before and after emulsification (using UV–visible spectrophotometry) to estimate Γ_{ads} . For appropriate samples, the thin sheet analysis (also called the Kratky–Porod or modified Guinier analysis) was performed as an internal consistency check on the polydisperse core/shell fitting approach, specifically the film thickness and resulting asphaltene composition of the film ($\phi_{\text{Asph, film}}$) determined by

$$\Gamma_{\text{Asph}} = \rho_m \phi_{\text{Asph, film}} \Delta_{\text{film}} \quad (5)$$

where Γ_{Asph} is the asphaltene surface mass concentration and ρ_m is the mass density of the asphaltenes (1.1 g/cm³). The assumption inherent in eq 5 is consistent with that which is imposed throughout the entirety of the study, that is, that the composition is uniform throughout the entire thickness of the film.

In addition to the film-only scattering approximation, an approximation of the surface scattering of the droplets was used when the samples were not contrast-matched, specifically in the second investigation in our study. The specific surface area is a property that can be extracted from a special contrast case such as that in

Figure 1d. We define this term as the total emulsion surface area, S , per unit sample of volume, V . Evaluation of the (S/V) term from neutron scattering data is derived from Porod's scattering laws.⁷⁰ The first of Porod's laws states that the total scattering from a system is a constant, C :

$$C = \int_0^\infty I(Q) Q^2 dQ = 2\pi^2 V (\Delta\rho)^2 \quad (6)$$

where V is the total volume through which the beam passes and $(\Delta\rho)^2$ is the square of the difference between the emulsion droplet and the bulk solvent phase SLD values. Porod's second scattering law states that the scattering from a sample will asymptotically approach a Q^{-4} dependence at high- Q , relative to some characteristic dimension, D , of the scatterer ($Q \gg 1/D$). Therefore, a plot of I^*Q^4 vs Q will asymptotically plateau at high- Q , provided the incoherent scattering is completely removed, which is not always the case. However, the value of the plateau is related to the specific surface area by

$$\left(\frac{S}{V} \right) = \pi \frac{P_{\text{Porod}}}{C} = \frac{P_{\text{Porod}}}{2\pi(\Delta\rho)^2} \quad (7)$$

where P_{Porod} is the plateau value of the I^*Q^4 vs Q plot. Generally, for nanoscopic scatterers, this plateau appears at $Q > 0.1 \text{ \AA}^{-1}$, but for our microscopic emulsions droplets the Porod Q^{-4} regime begins below the low- Q limit for SANS due to the large dimensions ($> 10\,000 \text{ \AA}$) of the droplets. The high- Q regime, as described earlier, can be used to assess the incoherent background scattering using the slope of an I^*Q^4 vs Q^4 plot. We found that converting the data to the I^*Q^4 plot leads to higher relative error, both in the data and the resulting analysis. For this reason, we fitted the absolute $I(Q)$ data with the following function:

$$I(Q) = P_{\text{Porod}} Q^{-4} + \text{bkg} \quad (8)$$

The resulting P_{Porod} value from the fit, which will herein be referred to as the Porod slope, is used along with eq 9 for evaluation of the sample S/V .

Ideally, the specific surface area could be used to ascertain the emulsion droplet size. Assuming the droplets have spherical geometry and are monodisperse, then the specific surface area simply becomes

$$\left(\frac{S}{V} \right) = \frac{3\phi}{R_{\text{drop}}} \quad (9)$$

where ϕ is the volume fraction of droplets and R_{drop} is the radius of the droplets. However, microscopic observations indicate that the droplets are significantly polydisperse and can be adequately described by a Schultz distribution (cf. Supporting Information). When applying the Schultz formalism to the droplet size distribution, a modified form of eq 9 is recovered:

$$\left(\frac{S}{V} \right) = \frac{3\phi}{R_{\text{avg}}} \left(\frac{z+1}{z+3} \right) \quad (10)$$

where R_{avg} is the average droplet radius consistent with the distribution and z is the polydispersity index. The z term is defined as $(R_{\text{avg}}/\sigma_R)^2 - 1$, where $2\sigma_R$ is the full-width at half-maximum of the distribution. Note that eq 10 has two unknowns, R_{avg} and z , such that, without a complementary experiment to obtain either R_{avg} or z , it is not feasible to recover both R_{avg} and z from only the Porod slope. Regardless, eq 10 will prove to be useful in the application of the core/shell form factor modeling.

For the form factor modeling analysis, we opted to use the core/shell model of Bartlett and Ottewill.⁷¹ Their geometric description

(67) King, S.; Griffiths, P.; Hone, J.; Cosgrove, T. *Macromol. Symp.* **2002**, *190*, 33–42.

(68) Hone, J.; Cosgrove, T.; Saphiannikova, M.; Obey, T.; Marshall, J.; Crowley, T. *Langmuir* **2002**, *18*, 855–864.

(69) Cosgrove, T.; Hone, J.; Howe, A.; Heenan, R. *Langmuir* **1998**, *14*, 5376–5382.

(70) Glatter, O.; Kratky, O., Eds. *Small-Angle X-ray Scattering*; Academic Press: London, 1982.

(71) Bartlett, P.; Ottewill, R. H. *J. Chem. Phys.* **1992**, *96*, 3306.

involves core/shell type spherical scattering bodies, where the core radius is described by the Schultz distribution and the shell thickness is constant. The description also includes the SLDs for the aqueous core, interfacial film, and organic bulk phases. In all, the model, for which a schematic is shown in Figure 1e, consists of 8 inputs: ϕ_{drop} , R_{avg} , p , Δ_{film} , ρ_{core} , ρ_{film} , ρ_{bulk} , and I_{bkg} . For this work, ϕ_{drop} is the emulsion droplet volume fraction, R_{avg} is the average core radius, p is equivalent to σ_R/R_{avg} from the droplet size distribution, Δ_{film} is the film thickness, ρ_i is the scattering length density of phase i , and I_{bkg} is residual incoherent background scattering. Scattering length densities for the materials used in the solvent dependence investigation are available in the Supporting Information. With knowledge of the aqueous phase SLD, droplet size distribution, droplet volume fraction, and subtraction of the incoherent background contribution, only the film and bulk phase SLD terms, as well as the film thickness, were the required fitted parameters. From the film SLD, we then calculated the asphaltene fraction in the film ($\phi_{\text{Asph, film}}$) using a volume fraction weighting of the asphaltene and matched aqueous/solvent SLD values. The resulting asphaltene surface concentration was computed by eq 5, using this $\phi_{\text{Asph, film}}$ and Δ_{film} recovered from the core/shell analysis.

In the latter investigation in this study, regarding aqueous phase pH variation and ACA addition, the film SLD term was replaced with a volume fraction weighted sum of the individual components that make up the film:

$$\rho_{\text{film}} = \phi_{\text{Asph, film}} \rho_{\text{Asph}} + \phi_{9\text{-ACA, film}} \rho_{9\text{-ACA}} + \phi_{\text{Tol, film}} \rho_{\text{Tol}} + \phi_{\text{Wat, film}} \rho_{\text{Wat}} \quad (11)$$

where $\phi_{X, \text{film}}$ and ρ_X are the volume fraction in the film and scattering length density of component X , respectively. Along with the condition that $\sum \phi_{X, \text{film}} = 1$, eq 11 directly incorporates the entire film composition into the core/shell model. For each unique emulsion condition (i.e., pH and ACA content), we prepared several chemically identical samples that differed only in the degree of deuteration. Our supposition is that samples prepared under identical conditions yield emulsions with identical properties. Thus, we employed a simultaneous fitting routine, in which several “global” model parameters were shared among the chemically identical samples for a given condition (e.g., pH 7, no ACA). Only two or three parameters, depending on ACA addition, were considered “local” parameters in a contrast variation series: ρ_{Tol} , ρ_{Wat} , and, when applicable, ρ_{ACA} . All local parameters were held constant during model fitting, with their values depending on the degree of deuteration. Of the global parameters, p , ϕ_{drop} , Δ_{film} , and ρ_{asph} were held constant during fitting; the rest, however, were allowed to vary. Figure 2 depicts the parameter types and their roles during simultaneous model fitting in the investigation pertaining to pH variation and ACA addition.

Simultaneous fits were optimized by minimizing the sum of the reduced chi-squared terms from all six samples in a contrast variation series:

$$\sum \chi_{\text{red}}^2 = \sum_j \left(\frac{\sum_i \left(\frac{I_{\text{CS}, i} - I_{\text{data}, i}}{\delta_{I, i}} \right)^2}{n_{\text{pts}} - n_{\text{params}} + n_{\text{fixed}}/j} \right) \quad (12)$$

where I_{CS} and I_{data} are the scattering intensity from the core/shell model and the data, respectively, δ_i is the statistical error on the data, n_{pts} is the total number of data points for a sample, n_{params} is the total number of parameters in the model, and n_{fixed} is the number of parameters held constant during fitting. The average χ_{red}^2 values reported later in the text are simply the summation in eq 12 divided by the number of samples (six) in the summation. To be consistent, core/shell model fits were performed over the same Q range as the thin sheet fits (0.004–0.04 \AA^{-1}).

Emulsion Stability to Centrifugation. Three emulsions were prepared with a 1:1 (v/v) mixture of 1% NaCl in D₂O/1% HOW in hydrogenated toluene, 1-methylnaphthalene, or decalin and aged 24 h. After resuspension, each emulsion was transferred into three individual graduated microcentrifuge tubes with 1.75 mL of emulsion

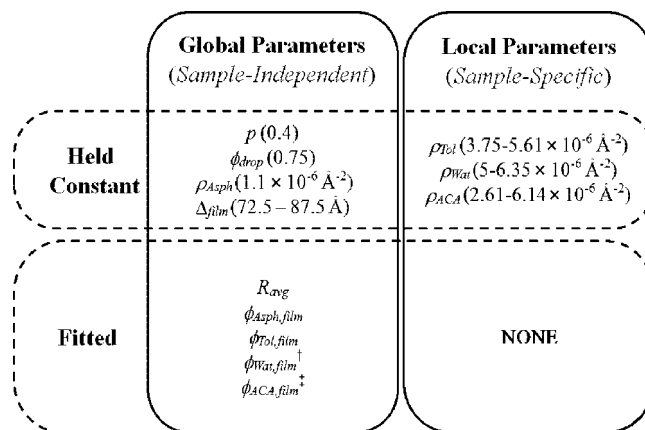


Figure 2. Core/shell form factor model parameters and how they are treated during simultaneous fitting in the pH/ACA investigation. Global parameters are those that are equivalent among all samples in a given contrast variation series (e.g., HOW-only emulsions at pH 7). The droplet volume fraction, asphaltene SLD, film thickness, and droplet polydispersity are the only global parameters held constant during fitting, while the rest are fitted as part of the optimization. Local parameters are those that differ among samples in a contrast variation series, and no local parameters were fitted. [†] $\phi_{\text{Wat, film}} = 1 - \phi_{\text{Asph, film}} - \phi_{\text{Tol, film}}$ in HOW-only samples, but fitted in ACA-added samples. [‡] $\phi_{\text{ACA, film}} = 1 - \phi_{\text{Asph, film}} - \phi_{\text{Tol, film}} - \phi_{\text{Wat, film}}$ in ACA-added emulsions.

in each tube. Using an Eppendorf MiniSpin Plus microcentrifuge, the samples were centrifuged at 14 500 rpm (RCF = 14 000g) for 1 h at room temperature. The volume of water resolved was determined by visual inspection, followed by pipet removal and weighing for verification. The percentage of water resolved due to centrifugation was calculated by

$$\% \text{ resolved} = \frac{V_{\text{res}}}{\phi_{\text{w}} V_{\text{em}}} \times 100 \quad (13)$$

where V_{res} is the volume of water resolved by centrifugation, ϕ_{w} is the volume fraction of water in the emulsion (~ 0.5 here), and V_{em} is the total volume of the emulsion sample (1.75 mL here).

Droplet Tensiometry. In the solvent dependence study, interfacial dilatational rheology was performed using a Tracker-H oscillating pendant drop tensiometer from Teclis (formerly I.T. Concept). The model oil phase was 1% (w/w) HOW asphaltenes dissolved in toluene, decalin, or 1-methylnaphthalene. The water phase was DI water adjusted to pH 7 using dilute NaOH and HCl. The drops were prepared using an 18-gauge stainless steel curved needle to allow the oil to rise in the surrounding aqueous medium. A description of the instrument is provided elsewhere.³² The drop volume for each system was 25 μL , with 2.5 μL applied volume oscillations having a frequency of 0.1 Hz. For each system, the aging time was 20–24 h, with sustained oscillations administered in 100 s increments once every hour.

In the pH and ACA dependence study, solutions were prepared in toluene with 2 mM 9-ACA, 1% (w/w) HOW, or a 1% (w/w) HOW and 5 mM 9-ACA mixture, 1% and contacted with a 1% (w/w) NaCl solution in deionized H₂O at pH 7 and 10. Interfacial tension measurements were recorded over the duration of 1 h of interfacial aging. A 250 μL glass syringe was used to house the oil phase, and it was equipped with a curved 20-gauge, flat-tipped, stainless steel needle. The drop volume was 25 μL , and the instrument was set to maintain a constant area using PID control. All experiments were performed at room temperature, which typically was 21 ± 3 °C.

Results and Discussion

Investigation I: Solvent Dependence of Emulsion Film Properties. SANS of Nonrinsed Emulsions. Accounting for aggregate scattering of nonrinsed emulsion samples was performed post-experimentally, as previously described. This is

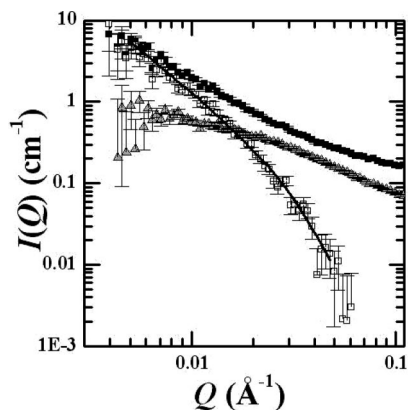


Figure 3. Accounting for aggregate contributions to emulsion scattering (black squares) by subtraction of ϕ -weighted creamed oil scattering (gray triangles). The final aggregate-subtracted data (open squares) are fitted with a polydisperse core/shell model (solid black line) to obtain the film thickness and scattering length density.

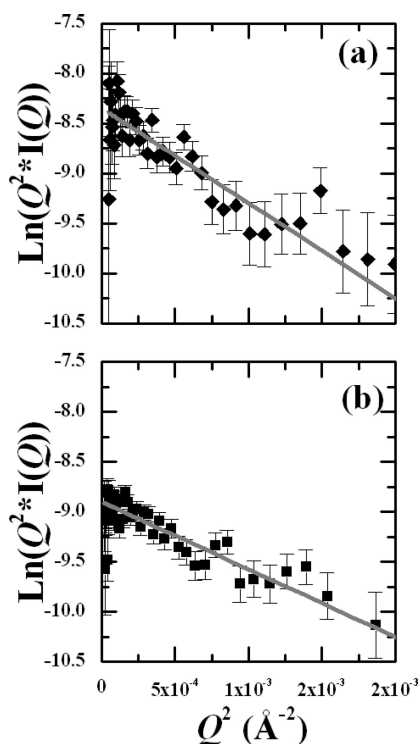


Figure 4. Kratky–Porod linearizations for nonrinsed emulsions made with 1% (w/w) HOW in (a) 1-methylnaphthalene and (b) toluene. These emulsions were aged for at least 24 h before being resuspended and transferred to the sample cell and scattered on the SAND instrument at ANL. Aggregate scattering and background were subtracted using eq 1 in the text prior to the linearization.

shown in Figure 3, which highlights the individual parts that comprise the nonrinsed emulsion $I(Q)$ data collected at ANL. As was typically the case, the core/shell model fit the aggregate/solvent/water-subtracted scattering data very well. Additionally, Figure 4 reveals the relative error that remains when one performs such subtractions. Each subtraction step retains the absolute error from the total emulsion scattering, and if the aggregate and interfacial film scattering have comparable intensity, the final relative error can be very significant. Despite this concern, for most samples, this approach yielded reasonable and believable fit parameters when applying the core/shell model. The plots in Figure 4 demonstrate the linearity of the Kratky–Porod (KP) evaluations over the appropriate Q^2 range, which is comparable

to what has been reported for other systems.^{58,60,72} For each emulsion scattered, the resulting film thickness and asphaltene composition in the film from the KP analyses and core/shell model fitting are compared in Table 2. To elaborate on the sample nomenclature, MN, T, and D represent emulsions made in *d*-methylnaphthalene, *d*-toluene, and *d*-decalin solutions, respectively. The -1 h, -1 d, and -2 d designations indicate the aging time, in hours and days, respectively, of the emulsion prior to the scattering measurement. The D1 and D2 samples were two decalin emulsions created under identical conditions but measured separately for reproducibility purposes.

For samples where such a comparison was appropriate, the Kratky–Porod analyses agreed well with the core/shell model, within the error of their calculations. However, for the samples prepared using decalin, there was almost a 15% discrepancy between the SLD of *d*-decalin ($7.27 \times 10^{-6} \text{ \AA}^{-2}$) and the 1% NaCl in D₂O solution ($6.36 \times 10^{-6} \text{ \AA}^{-2}$). Core/shell model calculations made using SLDs this offset from the contrast-matched condition show a marked deviation in the low- Q portion of the intensity data from a slope of -2 toward -4 on a log–log plot. This rendered the Kratky–Porod approximations and subsequent calculations invalid. It also suggested that the low- Q scattering signal was becoming dominated by the droplet scattering (Q^{-4}), which made it increasingly difficult to simultaneously recover both the film thickness and SLD. This arises from the low relative volume fraction of the interfacial films to that of the droplets, that is, $\phi_{\text{film}}/\phi_{\text{drop}}$. For a system with a $3 \mu\text{m}$ average radius, $p = 0.5$, and $\Delta_{\text{film}} = 100 \text{ \AA}$, this $\phi_{\text{film}}/\phi_{\text{drop}}$ equals 0.0075, indicating the film volume fraction is less than 1% of the droplet volume fraction. Thus, even small SLD differences can lead to a droplet-dominated signal at low- Q .

SANS of Rinsed Emulsions. Unlike their nonrinsed counterparts, rinsed emulsions yielded data devoid of aggregate scattering, which enabled evaluation of our contrast-matching abilities. This concept becomes clearer with Figure 5, which depicts a contrast variation experiment where the H₂O/D₂O composition of the water phase was varied, while the continuous phase consisted of fresh *d*-toluene per the aforementioned solvent replacement protocol. In Figure 5b, the intersection of the tangent lines to the low- Q scattering intensity as a function of aqueous phase D₂O composition indicates a minimum between 87 and 89% (v/v) D₂O. This composition corresponds to the core/bulk contrast-matched condition, at which the core aqueous and bulk solvent phases have equivalent SLD values, rendering the two phases indistinguishable in a SANS experiment. In these emulsion systems, it is possible to isolate the scattering that arises from the interfacial film material, alleviating ambiguity in the analysis. However, the narrow aqueous phase composition window for this contrast-matched condition would require volumes ~ 100 – 1000 times larger than what we prepared in order to accurately control the SLD to make a *perfectly* contrast-matched sample. Regardless, our analyses indicate the average SLD discrepancy between the aqueous and organic solvent phases for most samples was sufficiently small to treat the samples as contrast-matched.

As a follow-up, we tested the effects of rinsing on the fitted parameters using decalin and toluene as solvents for HOW asphaltenes. As deuterated solvents are expensive, hydrogenated solvents were used for the first three to five rinses, followed by an additional series of three to five replacements with deuterated solvent. The core/shell and Kratky–Porod fitting results of this investigation are presented in Table 3, specifically the properties of the interfacial films and how they depend on the solvent used,

(72) Knoll, W.; Haas, J.; Stuhmann, H. B.; Fuldner, H. H.; Vogel, H.; Sackmann, E. *J. Appl. Crystallogr.* **1981**, *14*, 191.

Table 2. Characteristic Core/Shell and Kratky–Porod Description of Nonrinsed Emulsions Prepared in Toluene-*d*₈, 1-Methylnaphthalene-*d*₁₀, and Decalin-*d*₁₈^a

sample ID	aging time	ϕ_d	core/shell analysis				Kratky–Porod		
			Δ_{film} (Å)	ρ_{film} ($\times 10^{-6}$ Å ⁻²)	$\phi_{\text{Asph, film}}$	χ^2_{red}	Δ_{film} (Å)	$\phi_{\text{Asph, film}}$	χ^2_{red}
MN-1 h	1 h	0.50	108 ± 5	5.36 ± 0.02	0.14	1.1	118 ± 6	0.13	1.1
MN-1d	24 h	0.50	99 ± 4	5.21 ± 0.03	0.17	0.8	107 ± 5	0.16	0.7
T-1 h	24 h	0.55	83 ± 4	4.65 ± 0.03	0.21	0.8	91 ± 5	0.20	0.8
T-2d	50 h	0.50	85 ± 3	4.84 ± 0.02	0.17	1.4	90 ± 3	0.13	1.4
D1-1d	24 h	0.53	45 ± 1	3.99 ± 0.05	0.53	2.3			
D2-1d	24 h	0.53	41 ± 1	3.96 ± 0.05	0.54	4.2			

^a Emulsions were prepared with a composition of 1:1 (v/v) model oil/1% NaCl solution.

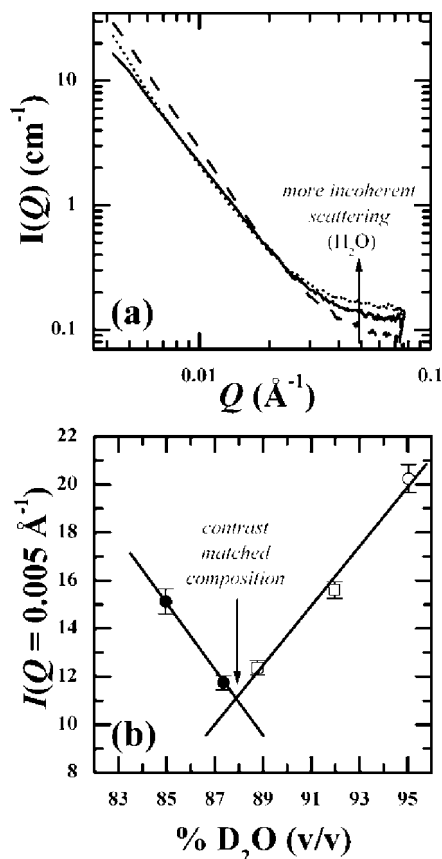


Figure 5. (a) Rinsed emulsion scattering curves for contrast variation of toluene-based emulsion samples with 95% (dashed line), 87% (solid line), and 85% (dotted line) D₂O in the aqueous phase. (b) Scattering intensity at $Q = 0.005 \text{ \AA}^{-1}$ as a function of aqueous phase D₂O concentration. Filled data points (black circles) represent samples of deuteration below the contrast-matched condition ($\text{SLD}_{\text{aqueous}} < \text{SLD}_{\text{bulk}}$), and vice versa for unfilled points (white squares and circles). Circles refer to the compositions shown in (a). The minimum, estimated here by intersecting extrapolated linear fits to the data, indicates the contrast-matched point is nearly 88% D₂O/12% H₂O.

the rinsing protocol, and bulk asphaltene concentration. To clarify the sample ID nomenclature, D1 and D2 are two separate HOW in decalin emulsion samples prepared under identical conditions. They were each rinsed five times with *h*-decalin followed by three rinses with 87:13 *d*:*h*-decalin. For the D1-Repeat sample, we simply repeated the scattering measurement without removing the sample from the scattering cell. In D2-XR, we performed an additional four 87:13 *d*:*h*-decalin rinses. We again performed the scattering measurement on D2-XR for repeatability purposes, but we waited 7 h to test the impact of aging after solvent replacement, which is represented by D2-XR+7 h. For rinsed toluene-based emulsions, T1 and T2 were identically prepared HOW emulsions, with the -XR representing the samples that underwent an additional four *d*-toluene rinses.

Small changes in core/shell fitted parameters suggest the solvent replacement protocol was not disruptive. First, modest changes in the film thickness were observed with subsequent repeated measurements, postrinsing aging, and additional rinsing; the D2 and D2-XR series was the most obvious exception. Additional solvent replacements typically led to core/shell fits of slightly higher χ^2_{red} , indicating lower fit quality. However, this is not always a good *comparative* measure, as some data have higher count rates and thus smaller statistical errors, leading to larger χ^2_{red} calculations. The most noticeable changes upon additional deuterated rinses are in the scattering length densities for both the interfacial film and the bulk solvent. For samples in which the rinsing was insufficient to replace all of the free solvent, the SLD of the solvent was a fitted parameter. In samples having undergone further rinsing steps, the solvent SLD was fixed at a value calculated using estimates of the residual bulk solvent remaining after each replacement. For both the toluene and decalin series, the solvent SLD after the first set of deuterated rinses was lower than that of the replacement solvent by 3–15%, respectively. Increases in the film SLD with additional rinses were also recovered during our core/shell fitting analyses. For the decalin emulsions, the film SLD increased 7% from nearly 4.2×10^{-6} to $4.7 \times 10^{-6} \text{ \AA}^{-2}$ with an extra four solvent replacements using the 87:13 *d*:*h*-decalin mixture. Increases in the film SLD for the toluene emulsions were less noteworthy, equating to about 1–2%. Computation of the asphaltene volume fraction in the films from the film, bulk, and asphaltene SLDs indicated that $\phi_{\text{Asph, film}}$ did not vary significantly with rinsing.

From these results arise three inferences: (1) the asphaltenic material in the films is stable to rinsing and thus nearly irreversibly adsorbed, (2) the asphaltene composition in the film demonstrates a dependence on the aromatic and aliphatic character of the solvent, and (3) solvent is present along with asphaltenes in the interfacial films and is free to exchange with the bulk. Some of these observations are not novel. For example, it has been reported that after asphaltenes adsorb and undergo interfacial rearrangement, little or no desorption occurs after replacement of the bulk phase with fresh solvent.^{24,27,73} Additionally, using a Langmuir trough, Ese et al. used Π -*A* isotherms to calculate asphaltene surface concentrations as a function of the hexane/toluene ratio in a mixed solvent for three different asphaltenes, for which they observed a general increase in the asphaltene surface concentration with increasing hexane concentration.²³ This is consistent with our observations of larger $\phi_{\text{Asph, film}}$ from HOW-stabilized rinsed emulsions in alicyclic decalin (~30%) compared to those in aromatic toluene (~12%). However, to our knowledge, this is the first time anyone has evaluated the asphaltenic composition in interfacial films based solely on SANS data and model analyses, rather than relying on a difference analysis based on the bulk phase properties. This is the key advantage of this interfacial probing technique, which does not require imposition of an

(73) Freer, E. M.; Radke, C. J. *J. Adhes.* **2004**, *80*, 481.

Table 3. Characteristic Core/Shell Parameter Description of Rinsed Emulsions Prepared in Toluene- d_8 and Decalin- d_{18} ^a

sample ID	hydr. rinses	deut. rinses	core/shell analysis					Kratky–Porod		
			$\rho_{\text{solv}} (\times 10^{-6} \text{ \AA}^{-2})$	$\Delta_{\text{film}} (\text{ \AA})$	$\rho_{\text{film}} (\times 10^{-6} \text{ \AA}^{-2})$	$\phi_{\text{Asph, film}}$	χ^2_{red}	$\Delta_{\text{film}} (\text{ \AA})$	$\phi_{\text{Asph, film}}$	χ^2_{red}
D1	5	3	5.53 ± 0.01	91 ± 1	4.25 ± 0.02	0.29	2.5			
D1-Repeat	5	3	5.55 ± 0.01	92 ± 1	4.28 ± 0.02	0.29	4.0			
D2	5	3	5.40 ± 0.01	90 ± 1	4.17 ± 0.02	0.29	2.5			
D2-XR	5	7	6.31	100 ± 1	4.72 ± 0.01	0.31	8.4	107 ± 1	0.29	6.14
D2-XR-7 h	5	7	6.31	98 ± 1	4.65 ± 0.01	0.32	10.1	104 ± 1	0.30	7.68
T1	3	5	5.46 ± 0.01	91 ± 3	4.99 ± 0.01	0.11	0.6			
T1-XR	3	9	5.6	98 ± 2	5.07 ± 0.01	0.12	2.6	104 ± 2	0.11	2.18
T2	3	5	5.47 ± 0.01	101 ± 2	4.98 ± 0.01	0.11	1.2			
T2-XR	3	9	5.6	104 ± 2	5.04 ± 0.01	0.13	1.7	111 ± 2	0.12	1.41

^a Emulsions were prepared with a composition of 50:50 (v/v) model oil/1% NaCl solution.

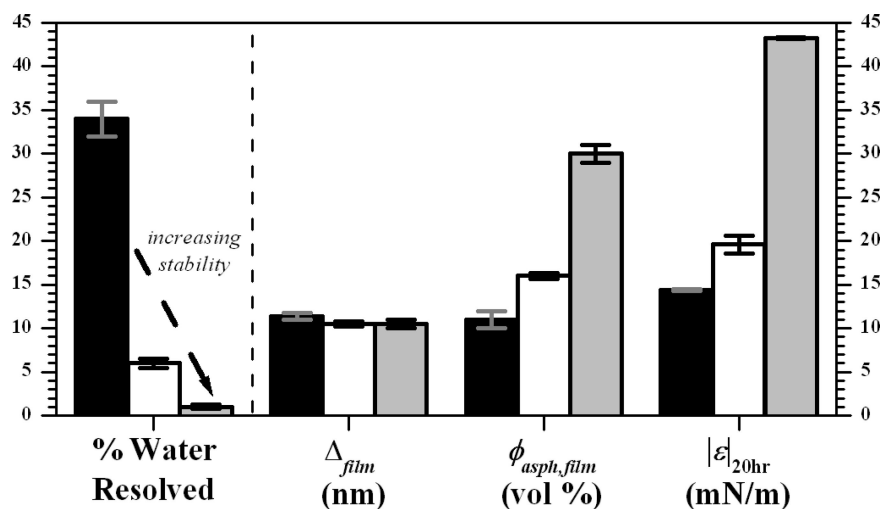


Figure 6. Comparison of results from centrifugation, SANS, and interfacial rheology for HOW-based model oil/water interfaces for three different cyclic hydrocarbon solvents. Toluene (black), 1-methylnaphthalene (white), and decalin (gray) were the solvents used. The vertical dashed line separates properties of the emulsion (left) and those of the interfacial film.

interfacial geometry any different from the native emulsion. Additionally, we deduced that the films were not entirely composed of a dense asphaltene arrangement; rather, they were swollen with solvent and possibly water. This was consistent with previous SANS investigations that have reported the entrainment of the host solvent(s) within bulk asphaltenic aggregates.^{53,56} We pursue a more encompassing description of the film composition (water, solvent, and additive) in the latter investigation in this text.

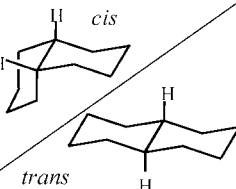
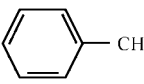
Emulsion Stability. Shown in Figure 6 is a comparison of analyses from the centrifugation, neutron scattering, and interfacial rheology experiments. With decreasing water resolution by centrifugation, the emulsion stability is said to increase in the order toluene, 1-methylnaphthalene, and decalin. From this chart, it is clear that while asphaltenic film thickness did not trend with the degree of water resolution after centrifugation, both the film asphaltene composition and long-time dilatational modulus increased accordingly with increasing emulsion stability. These observations suggest that, for HOW-stabilized emulsions, the predominant contributor to emulsion stability was the composition of asphaltenes within the interfacial film. This likely had to do with the strong associative behavior of the HOW asphaltenes, which also have significant polar heteroatom (N, S, and O) composition as indicated in Table 1. From polydisperse oblate cylinder (POC) fits of SANS data for HOW solutions in the three solvents used here, we observed increases in the average radius of gyration and volume of HOW aggregates in the series 1-methylnaphthalene, toluene, and decalin (cf. Table 4). Conversely, Table 4 demonstrates a decrease in the degree of solvent entrainment within aggregates in the same order of solvents.

Given the larger and denser aggregates (lower solvent entrainment) in decalin compared to toluene and methylnaphthalene, it logically follows that the interfacial films in decalin emulsions would also be richer in asphaltene than films from emulsions in either toluene or methylnaphthalene. However, the applied oblate discoidal shape implies the aggregate size discrepancies are generally in the radial direction. Provided the films consist of asphaltene multilayers formed by adsorbed aggregates, as has been suggested in the literature,^{12,22,74} and these aggregates stack and overlap on the interface between their top and bottom faces, then observed film thickness values between 80 and 130 Å suggest these multilayers consist of loosely packed stacks of four to seven aggregates. This is based on the aggregate thickness from POC fits, which roughly fell between 15 and 26 Å for 1% (w/w) HOW in methylnaphthalene, toluene, and decalin.⁵⁶

Validity of Analyses. It can be expected that the core/shell model is an idealized version of an emulsion droplet, particularly in two central assumptions that (1) the film thickness is constant throughout the entire population of droplets and (2) the film boundaries are sharp interfaces. While these are plausible contentions to the core/shell model of Bartlett and Ottewill,⁷¹ the use of this model for our systems is defensible. First, decoupling the manifestations of film thickness and droplet size polydispersity from data such as these is not straightforward. In the least, assuming constant film thickness over all of the droplets yields an average value for the film. In fact, these thicknesses seem to correspond well with those reported from the aforementioned

(74) Jeribi, M.; Almir-Assad, B.; Langevin, D.; Henaut, I.; Argillier, J. F. *J. Colloid Interface Sci.* **2002**, *256*, 268.

Table 4. Characteristic Properties of the Solvents Used and Their Resulting HOW Aggregates^{a,b}

Solvent Properties	Property	Decalin	Toluene	1-Methylnaphthalene
	Chemical Structure			
	$\delta_D, \delta_P, \delta_H$ ($J^{0.5}/cm^{1.5}$)	18.4, 0, 0	18, 1.4, 2	20.6, 0.8, 4.7
	η (cP)	2.03-3.23	0.59	3.12
Aggregate Properties	R_G (Å)	72	56	47
	V_{POC} (nm^3)	267	128	65
	$\Phi_{\text{entrainment}}$ (% v/v)	27	36	40

^a The solvents are listed left to right in increasing aromatic character. ^b From reference 56.

SANS work of Jestin et al.⁶⁵ (110–150 Å) as well as Langmuir–Blodgett/AFM-determined interfacial thickness for adsorbed asphaltenic film structural features (10–13 nm).³⁷ So, while including a polydispersity term for the film thickness may be applied in future work, it will likely require very accurate knowledge of the droplet distribution for the film thickness distribution to be of any value. In this investigation, we used optical microscopy, which could not capture droplets substantially smaller than 1 μm in diameter and where the sample populations were only a few hundred to a few thousand droplets at the highest magnification; the actual droplet population through which the neutron beam passes is several orders of magnitude greater.

With respect to the film boundary assumptions, we recognize that a diffuse film boundary can enhance the description of the system, but the value in expanding the complexity of our model is limited to the features in the scattering data that are affected by such expansion. The non-negligible polydispersity of the droplet distribution already smoothes out the periodic “humps” observed for nearly monodisperse scattering systems, leaving only the curvature and magnitude as the main characteristic “features” of the scattering data. Each of the eight inputs for the polydisperse core/shell model can impact either the curvature or magnitude of the model output. By limiting the number of these inputs that served as fitted parameters, we reduced the ambiguity surrounding those parameters. Finally, the quality of the fits from the core/shell and Kratky–Porod analyses, described partly by the χ^2_{red} term in Tables 2 and 3, is an indication that these models do describe the scattering well, particularly for contrast-matched data. However, we recognize that these are among the simplest descriptions of the scattering system, and should be expanded upon in future work to recover structural information *within* the film, particularly with respect to the asphaltene volume fraction profile, as has been documented for polymer layers on solid particle surfaces.^{67–69,75,76}

Investigation II: Aqueous pH Variation and Organic Acid Addition. *Comparison of Scattering Approximations and Core/Shell Modeling.* The goal of this investigation was to elucidate

Table 5. Compositional Information of the Contrast Variation Series for 3% HOW Emulsions at pH 7 and pH 10

emulsion ID	% of solvent that is:		% of water that is:	
	<i>d</i> -toluene	<i>h</i> -toluene	D ₂ O	H ₂ O
CV-A	60	40	100	0
CV-B	80	20	100	0
CV-C	100	0	100	0
CV-D	100	0	89	11
CV-E	100	0	80	20

Table 6. Composition Information of the Contrast Variation Series for 3% HOW/0.4% ACA Emulsions at pH 7 and 10

sample ID	% of solvent that is:		% of water that is:		% of ACA that is:	
	<i>d</i> -toluene	<i>h</i> -toluene	D ₂ O	H ₂ O	<i>d</i> -ACA	<i>h</i> -ACA
CV-1	60	40	89	11	100	0
CV-2	80	20	89	11	100	0
CV-3	100	0	89	11	100	0
CV-4	100	0	100	0	100	0
CV-5	100	0	80	20	100	0
CV-6	100	0	89	11	0	100

the specific interfacial area, the interfacial film thickness, and the compositional makeup of the interfacial films stabilizing water-in-model oil asphaltenic emulsions. We develop our analyses by describing HOW-only and then ACA-added model-oil emulsion results at pH 7 and 10. Two approximations are applied under specific contrast conditions to yield film thickness and the emulsion interfacial area per volume. These results agree with those from a more complex model that assumes core/shell geometry. By simultaneously fitting SANS scattering data from each series of chemically identical, yet isotopically distinct, emulsion samples, we then evaluate the individual component compositions within the films. Finally, we discuss the changes in the emulsion properties that occur with pH variation and ACA addition. To make clear the discussion surrounding the contrast variation samples for ACA-free and ACA-added emulsions, we have provided abbreviated emulsion identifiers in Tables 5 and 6, along with the relative deuteration of each component in the emulsion. The SLD values for various phases of the emulsions from Tables 5 and 6 can be found in the Supporting Information.

(75) Dale, P. J.; Vincent, B.; Cosgrove, T.; Kijlstra, J. *Langmuir* **2005**, *21*, 12244–12249.

(76) Cosgrove, T.; Heath, T. G.; Ryan, K. *Langmuir* **1994**, *10*, 3500–3506.

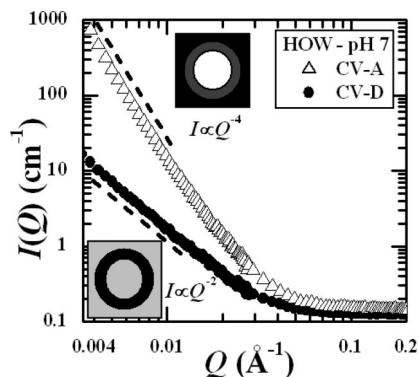


Figure 7. Manifestations of contrast variation in scattering for water-in-model oil emulsions. For the core/bulk contrast-matched condition (filled circles), when the organic phase consisted of perdeuterated toluene and the aqueous phase was 1% NaCl in 89:11 (v/v) D₂O/H₂O, that is, CV-D from Table 5, the resulting scattering approaches a Q^{-2} dependence at low- Q , consistent with film-only scattering. When the organic phase consisted of 60:40 (v/v) C₇D₈/C₇H₈ and the aqueous phase was 1% NaCl in D₂O (open triangles), that is, CV-A from Table 5, the resulting low- Q scattering approaches a Q^{-4} dependence, consistent with droplet-dominated scattering.

Two relevant special contrast conditions are those that result in either film-only (cf. Figure 1b) or droplet-only (cf. Figure 1d) scattering, which exhibit either Q^{-2} or Q^{-4} dependence at low- Q , respectively. Scattering behavior reminiscent of these two conditions is observed for the two samples in Figure 7, in which we show the absolute scattering intensity data for two pH 7 emulsions made from 3% HOW in toluene and 1% NaCl aqueous solutions. When the bulk phase consisted of perdeuterated toluene and the aqueous phase composition was 89:11 (v/v) D₂O/H₂O (black circles), that is, CV-D from Table 5, the aqueous phase SLD is very closely matched to that of the toluene phase, as discussed previously. The guideline in Figure 7 indicates that the data approach a Q^{-2} dependence at low- Q , indicative of thin sheet scattering. Also, for this core/bulk phase contrast-matched sample, the absolute intensity is rather low, on the order of 10 cm⁻¹. This is consistent with a low volume fraction of scattering components, in this case the volume fraction of interfacial film material throughout the sample. When the water phase was 1% NaCl in D₂O and the organic bulk phase was a 60:40 (v/v) blend of deuterated/hydrogenated toluene (open triangles), that is, CV-A from Table 5, the data clearly approach a Q^{-4} dependence at low- Q , consistent with Porod scattering from the droplet surface. As we will discuss later, this CV-A sample actually represents the contrast condition from Figure 1a, that is, all phases have a unique SLD. However, we will show that the SLDs of the film and the bulk phases are much closer to each other than the aqueous phase, and thus the contrast condition closely resembles Figure 1d. We note that the scattering intensity from this sample is several orders of magnitude greater in the low- Q range than the previous sample, reflective of a much higher volume fraction of scattering components, that is, droplets plus interfaces. The background value in intensity that occurs for $Q > 0.1$ Å⁻¹ is representative of the cumulative incoherent scattering from toluene, water, and asphaltene.

The plots in Figure 8 reflect the ability of thin sheet and Porod scattering approximations to fit the four sets of emulsions. Fits for background-subtracted data exhibiting Q^{-2} dependence at low- Q were performed using eq 2, where the I_0 and Δ_{TS} terms were allowed to vary. Asphaltene-only emulsions with this scattering behavior correspond to the CV-D designation from Table 5, while ACA-added emulsions carry the CV-3 designation from Table 6. For background-subtracted data exhibiting Q^{-4}

dependence at low- Q , fitting was performed using eq 8, with P_{Porod} being the only fitted parameter. Samples with this Q^{-4} dependence are labeled CV-A for HOW-only emulsions and CV-1 for ACA-added samples. For both special scattering approximations, the bkg term was fixed at 0 cm⁻¹ because of the aforementioned incoherent scattering subtraction protocol (using the slope of a Q^4I vs Q^4 plot). All thin sheet and Porod slope fits were performed in IGOR Pro by the minimization of the reduced χ^2 term. Each plot in Figure 8 stands as visual evidence of the good fitting quality for each approximation. However, as these are approximations, their validity holds only for samples that satisfy the appropriate contrast conditions.

The resulting film thickness and surface area evaluations from the fits shown in Figure 8 are provided in Table 7, along with the corresponding properties obtained from the core/shell model on the same samples; the agreement is excellent. Although the core/shell model can be considered a simple approximation of the emulsion sample, it offers significant additional detail beyond that of the thin sheet and Porod analyses, largely embedded in the film SLD. This is particularly important if the film is expected to have more than one component. The agreement in Table 7 between Δ_{TS} and $\Delta_{C/S}$ arises in part from the fact that, during fitting, we did not relax the assumption that the core and bulk SLDs were equivalent; they were both fixed at 5.61×10^{-6} Å⁻². Of note, the values for Δ_{TS} and $\Delta_{\text{film,C/S}}$ from these four series are roughly 20–30% less than what we previously recovered from 1% HOW in toluene emulsions and considerably lower than those for the 120–150 Å films reported by Jestin et al.⁶⁵ It is plausible that the thinner films here result from the adsorption of asphaltenes from a solution of higher concentration (3%) that leads to a denser film either due to more rapid adsorption or because of the chemical discrimination of the adsorbing species.

The results presented in Table 7 also indicate a decrease in the total droplet surface area per unit volume, S/V , with increasing pH, irrespective of the ACA content in the sample. For both pH conditions, we observe small but statistically significant decreases in S/V with ACA addition. For each of the four separate emulsion series, two evaluations of S/V are provided in Table 7. One was the result of the Porod scattering analysis (cf. eq 7) on the samples prepared with 60:40 *d:h*-toluene in the bulk phase (CV-A or CV-1 from Table 5 or 6). The other was calculated using eq 10 and R_{avg} from the simultaneous core/shell fits (recall p was fixed at 0.4 during the fits). The values for S/V calculated with the Porod slope were systematically larger than those calculated from the core/shell model fits. This discrepancy likely results from SLD mismatch between the bulk solvent and interfacial film. Analysis using the Porod slope assumes that contrast conditions are such that the film is indistinguishable from the bulk solvent, an assumption that is relaxed, but not ignored, when fitting with the core/shell model. Even relatively small mismatch of the bulk and film SLDs can lead to an overestimate of the Porod slope and thus a systematically larger S/V . Thus, the samples that are off-contrast and yield Q^{-4} scattering behavior at low- Q represent the contrast case of Figure 1a, but very close to that from Figure 1d. With this in mind, we describe the scattering from such samples as droplet-dominated rather than droplet-only. Overall, both S/V determinations yield values comparable to those (~4000 cm²/mL) recovered by optical microscopy in the solvent dependence investigation for samples with similar asphaltene surface coverage (decalin emulsions). Additionally, since the droplet population in a SANS measurement is several orders of magnitude greater than that in an optical microscopy measurement at high magnification (for better size

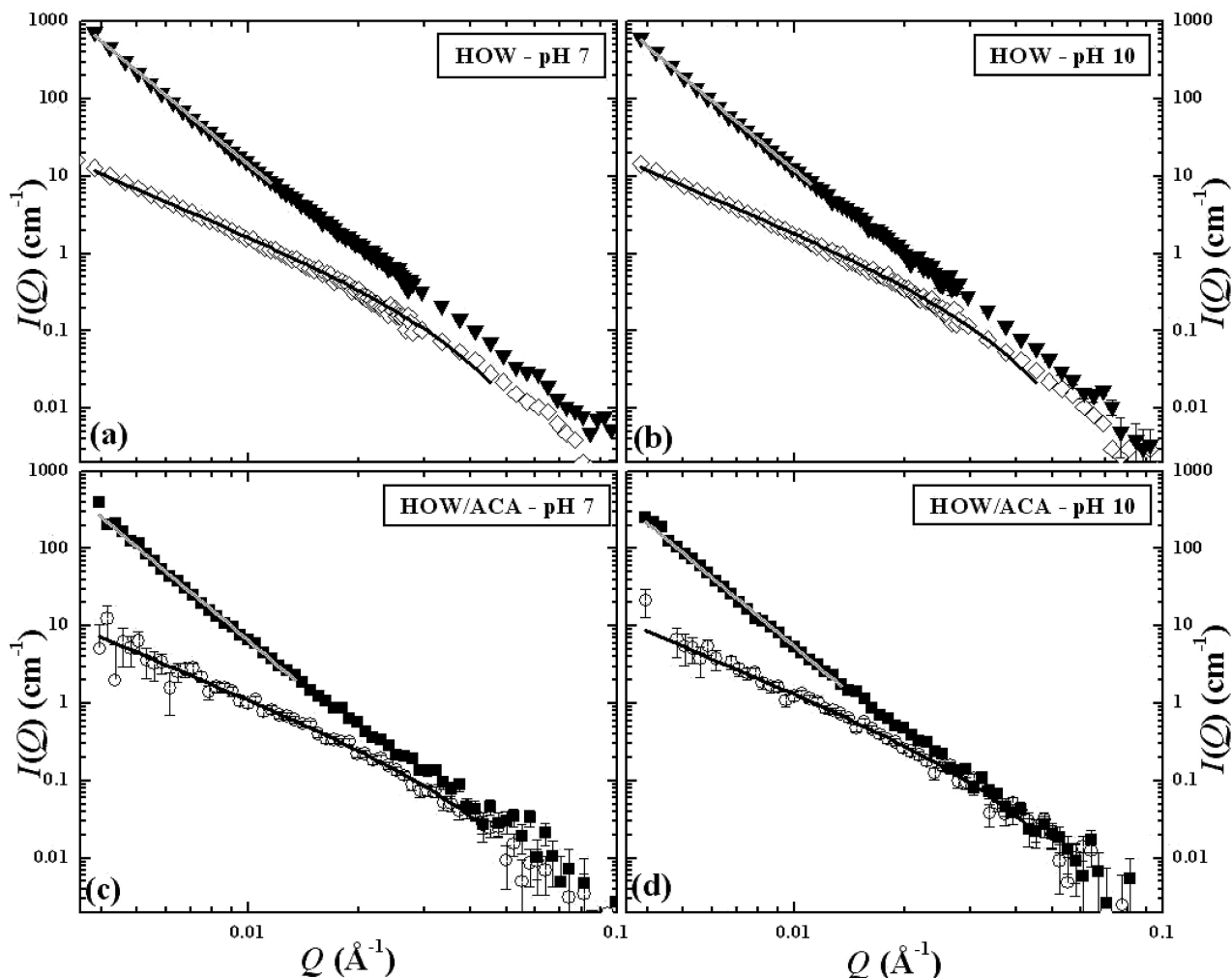


Figure 8. Emulsion samples made with (a,b) 3% HOW or (c,d) 3% HOW and 0.4% ACA in toluene. Open data points (pentagons and circles) designate samples with film-dominated scattering (CV-D and CV-3 conditions), while filled data points (inverted triangles and squares) correspond to droplet-dominated scattering conditions (CV-A and CV-1 conditions). Corresponding thin sheet fits (solid black lines) and Porod slope fits (solid gray lines) were performed using eqs 2 and 8, respectively.

Table 7. Film Thickness and Specific Surface Area Obtained from Special Contrast Cases (Thin Sheet and Porod Scattering) Compared to Values Recovered from Individual Core/Shell Fits of Relevant Samples in a Contrast Variation Series^a

emulsion identification	Δ_{TS} (Å) ^d	$\Delta_{film,C/S}$ (Å) ^d	S/V_{Porod} (cm ² /mL) ^e	$S/V_{C/S}$ (cm ² /mL) ^e
pH 7/3% HOW ^b	82 ± 5	84 ± 1	3383 ± 12	3057 ± 16
pH 10/3% HOW ^b	87 ± 5	88 ± 1	2877 ± 12	2622 ± 15
pH 7/3% HOW and 0.4% 9-ACA ^c	74 ± 5	71 ± 4	3074 ± 39	2763 ± 51
pH 10/3% HOW and 0.4% 9-ACA ^c	82 ± 5	79 ± 4	2563 ± 30	2320 ± 40

^a Results are shown for HOW-only and ACA-added emulsions made at pH 7 and pH 10. ^b Averaged from fits to NIST and ANL data. ^c Data collected at ANL. ^d From CV-D and CV-3 samples. ^e From CV-A and CV-1 samples.

resolution), the SANS-determined S/V is a reliable representation of the whole sample.

It is important to clarify that R_{avg} , not S/V , was the fitted parameter in the core/shell modeling. However, we observed that, for a given sample, independent of the fixed p value used in the model, the fitted R_{avg} value yielded identical S/V calculations made with eq 10. Thus, S/V was treated as the fitted parameter related to the drop distribution, for which comparative interpretation requires an independent measure of either the average droplet radius or polydispersity, or an assumption about the system polydispersity. More discussion on this issue can be found in the Supporting Information. A complement to SANS is ultrasmall-angle neutron scattering (USANS), which extends the low- Q range of SANS down to roughly $5 \times 10^{-5} \text{ \AA}^{-1}$, thus accessing larger scattering length scales. However, the average droplet

radii in the model emulsions studied here were too large to observe definitive characteristic features (i.e., the Guinier region) even at the lowest- Q of USANS. Future work may require implementation of techniques such as static light scattering or acoustic wave spectroscopy to complement SANS-based S/V determination.

Core/Shell Fitting: Interfacial Composition. The core/shell model is a simple but powerful description of our scattering system and is capable of unraveling interfacial film composition when coupled with controlled contrast variation experiments. Readers are directed to the Supporting Information for visualization of the core/shell fit quality and tables of the individual χ^2_{red} values for each sample. A complete list of results from the core/shell fitting is presented in Table 8, which includes film constituent compositions, S/V , and the average χ^2_{red} value. Values for R_{core}

Table 8. Resulting Fitted Parameters from Simultaneous Core/Shell Model for Each of Four Unique Emulsion Systems, Specifically HOW-Only and ACA-Added Emulsions at pH 7 and pH 10

	pH 7		pH 10	
	HOW	HOW/ACA	HOW	HOW/ACA
$\phi_{\text{Asph, film}}$	0.24	0.26	0.27	0.26
$\phi_{\text{Tol, film}}$	0.68	0.58	0.61	0.48
$\phi_{\text{Wat, film}}$	0.08	0.09	0.12	0.21
$\phi_{\text{ACA, film}}$		0.07		0.05
$\Delta_{\text{film}} (\text{\AA})^a$	83.0	72.5	87.5	80.5
$R_{\text{avg}} (\mu\text{m})$	5.5	6.1	6.4	7.2
$S/V (\text{cm}^2/\text{mL})$	3100	2800	2600	2400
avg χ^2_{red}	7.1	1.3	3.4	1.4
no. of samples in fit	6	6	6	6

^a Average of Δ_{TS} and Δ_{CS} from Table 7.

correspond to those that satisfy S/V when $p = 0.4$. When film thickness was allowed to vary during fitting, the fitted values of Δ_{CS} were much lower than those obtained only from the contrast-matched samples (cf. Table 7). This results from incorporation of contrast-mismatched samples, for which droplet surface scattering is of much greater intensity than that of the film. Thus, Δ_{CS} was held constant at the average thickness from the thin sheet and core/shell evaluations from Table 7, which had already demonstrated excellent agreement. Notably, although the footnote in Figure 2 identifies water and ACA as the film components chosen to satisfy the $\sum \phi_{X, \text{film}} = 1$ constraint during model fitting, the optimum composition was independent of this component designation. Using the film compositions from Table 8, the component SLDs, and eq 11, we illustrate in Figure 9 changes in film SLD for the 3% HOW-only emulsions at pH 7 (Figure 9a) and pH 10 (Figure 9b) as functions of either the water or toluene SLD. For reference, the core/bulk contrast-matched condition occurs where $\rho_{\text{Wat}} = \rho_{\text{Tol}} = 5.61 \times 10^{-6} \text{\AA}^{-2}$, at which resulting values for ρ_{film} were roughly $4.4 \times 10^{-6} \text{\AA}^{-1}$ at pH 7 and $4.3 \times 10^{-6} \text{\AA}^{-2}$ at pH 10. From eq 11, $\Delta\rho_{\text{film}}/\Delta\rho_X$ must be equivalent to the volume fraction of component X in the film ($\phi_{X, \text{film}}$). The highest slope on both plots in Figure 9 occurs for SLD changes in toluene, compared to those for water, indicative of solvent-rich films. Between pH 7 and 10, small changes in these slopes reflect the relative impact of pH on toluene and water film composition. Similarly, for the ACA-doped samples, ρ_{film} values are presented as a function of the individual component SLDs (cf. Figure 10). Again, the ρ_{film} dependence on the toluene SLD at both pH conditions is indicative of solvent-rich films.

Using eq 5 and $\phi_{\text{Asph, film}}$ from Table 8, the asphaltene surface concentrations from 3% HOW-only emulsions prepared at pH 7 and pH 10 were 2.2 and 2.6 mg/m², respectively. These values are roughly twice that of the 1% HOW-only emulsions prepared in toluene previously discussed, consistent with the larger bulk asphaltene concentration used here. This surface coverage agrees well with those recovered from tensiometry and gravimetry (1.4–3.9 mg/m²) for emulsions made with dilute athabasca asphaltene solutions (~0.1 wt %) in toluene and hexane/toluene mixtures.⁷⁷ Interestingly, Jestin et al.⁶⁵ reported similar surface coverages ($2.4 \pm 0.3 \text{ mg/m}^2$) for their dilute (0.3 wt % in xylene) C₇-asphaltene emulsions at pH 7 as well as a decrease (to $1.5 \pm 0.3 \text{ mg/m}^2$) when the pH was increased to 12 and 13. With ACA present at pH 7 and pH 10, the asphaltene surface concentrations actually decreased to 2.1 and 2.3 mg/m², respectively, mainly as a result of slightly thinner films than those for ACA-free emulsions with the same HOW concentration.

However, since Γ_{Asph} for a uniform film is directly proportional to the film thickness, it alone cannot provide information on how densely packed the film is with asphaltene. For example, a 100 Å thick film that is 50% asphaltenic will yield the same surface concentration as a 200 Å thick film that is 25% asphaltenic. This makes SANS an even more appealing interfacial characterization tool for asphaltenic emulsions, since one can resolve all of the following items: film asphaltene composition, film thickness, and total adsorbate surface concentration.

Overall, the film compositions provided in Table 8 offer a particularly comprehensive description of asphaltenic interfacial films. Additionally, these compositions were elucidated from data acquired using *only* SANS. Interestingly, the results suggest that, in addition to asphaltenes and solvent, the films also contain water. In fact, for HOW-only emulsions at pH 7, about 8% (v/v) of the interfacial film structure was determined to be aqueous. This film-based water most likely arises from an affinity to polar moieties of the asphaltenes at or near the film/water interface, for example, phenols, pyrroles, pyridines, and carboxylic acids. At pH 10, water composition increased to 12% (v/v) of the film, which may be the result of increased surface activity for acidic asphaltenic species, which is in line with the larger $\phi_{\text{Asph, film}}$ recovered at elevated pH conditions. When the acidic asphaltenic moieties adsorb to the oil/water interface, and the aqueous phase $\text{pH} > \text{p}K_{\text{a}}$ of the $-\text{COOH}$ group, equilibrium favors proton donation to the aqueous phase. This increase in film water composition may be necessary to maintain the deprotonated state of the resulting carboxylate ion, which has a high affinity for the briny water. This phenomenon is plausible, provided the adsorbed molecules are of sufficient size and/or overall chemistry to prevent them from completely traversing the interface into the alkaline aqueous phase, where they may be soluble. More simply stated, asphaltene molecules that are able to cross the interface will do so, while those that are too bulky to be soluble in the aqueous phase may actually draw water into the film. This behavior could continue with increasing pH until the water phase basicity/alkalinity warrants larger molecules to cross the interface and cause phase inversion, that is, O–W emulsions, or even O–W–O multiple emulsions.⁷⁸

A similar discussion arises when ACA is added to the system, as the polar $-\text{COOH}$ group provides a driving force for interfacial adsorption. However, larger and bulkier surface-active asphaltenes can exclude ACA from available adsorption sites and thus limit ACA inclusion presence at the film/water interface. From film composition changes with ACA addition at pH 7, the inclusion of ACA into the films corresponds with a partial exclusion of toluene from the film, with almost no change in water or asphaltene film composition. This implies that the ACA incorporation occurs uniformly throughout the film, adsorbed both as mixed HOW/ACA aggregates as well as free molecular monomers/dimers; that is, it is not concentrated near the film/water interface. Alternatively, at pH 10, the reduced toluene film volume fraction arises not only from ACA inclusion but also from an increased water volume fraction in the film. Again, this could be the result of an increased concentration of acidic species adsorbed directly at the film/water interface. This would suggest that at pH 10 ACA incorporation occurs primarily as free molecules adsorbed at the film/water interface, rather than mixed ACA/HOW aggregates uniformly distributed throughout the film.

These changes in ACA film composition with pH are consistent with changes in the protonation state of the acidic functional group. When the $-\text{COOH}$ group is uncharged, ACA is well

(77) Yarranton, H. W.; Hussein, H.; Masliyah, J. H. *J. Colloid Interface Sci.* **2000**, *228*, 52–63.

(78) Arla, D.; Sinquin, A.; Palermo, T.; Hurtevent, C.; Graciaa, A.; Dicharry, C. *Energy Fuels* **2007**, *21*, 1337–1342.

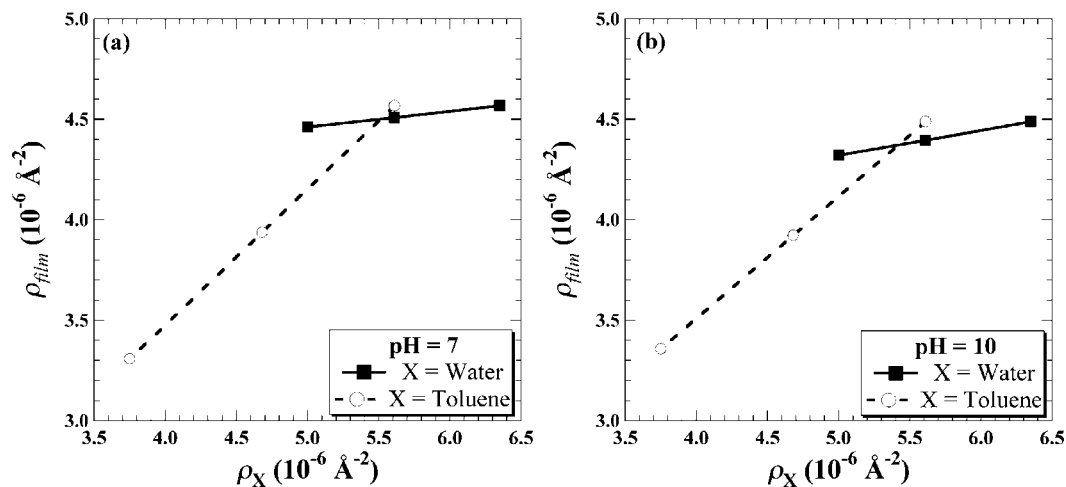


Figure 9. Impact of changes in water (filled squares) and toluene (open circles) SLD on the resulting film SLD from the core/shell model fitting for emulsions made with 1:1 (v/v) 3 wt % HOW in toluene solution and 1 wt % NaCl in water solution at (a) pH 7 and (b) pH 10.

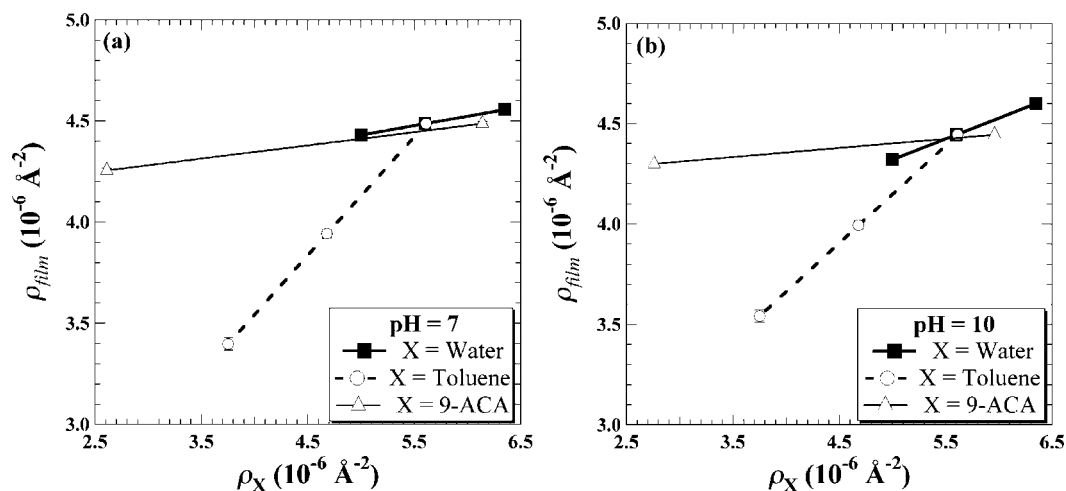


Figure 10. Impact of changes in water (filled squares), toluene (open circles), and 9-ACA (open triangles) SLD on the resulting film SLD from the core/shell model fitting for emulsions made with 1:1 (v/v) 3 wt % HOW/0.4 wt % 9-ACA in toluene solution and 1 wt % NaCl in water solution at (a) pH 7 and (b) pH 10.

solvated in the low dielectric constant medium of the film. At pH 10, where it is predominantly negatively charged, it is surface-active and thus cannot be embedded in the middle of the film. This rationale is consistent with the reduced $\phi_{\text{ACA, film}}$ reported in Table 8 at pH 10 compared to pH 7. Thus, even though the concentration of *interfacially active* ACA in the films at pH 10 was probably greater than that at pH 7, the overall film ACA composition was lower because these directly adsorbed ACA molecules occupy a smaller portion of the entire film than at pH 7.

These arguments are in accord with the dynamic interfacial tension profiles shown in Figure 11. The apparent band from 600 to 700 s is actually a series of oscillatory area deformations, which are normally used to evaluate interfacial viscoelasticity. Instead, the focus here was the time-dependent interfacial tension, which would be constant at 36.1 mN/m for a clean toluene/water interface.⁷⁹ The decaying dynamic interfacial tension profiles in

Figure 11a agree with those reported for asphaltenes and acidic petroleum species at neutral pH.^{74,80–84} Even at low bulk concentration, 9-ACA reduced the interfacial tension to 28 mN/m, while a solution of 1 wt % HOW asphaltenes reduced the tension to almost 24 mN/m. Mixtures of both 9-ACA and HOW asphaltenes appeared to reduce tension cooperatively, achieving a lower tension (19 mN/m) than either of the individual components at pH 7. This suggests that ACA acts not only as an asphaltene–asphaltene “binding agent,” as we previously hypothesized, but also as a tension reducing agent. However, the interfacial tension evolution profiles changed significantly at pH 10 (cf. Figure 11b). First, the minimum tension achieved for each sample was lower at pH 10 than at pH 7. This enhanced surface activity and tension reduction is consistent with the energetically favored deprotonation of the $-\text{COOH}$ groups on asphaltenes and ACA upon adsorption at the interface. Second, time-dependent features appear in all three systems: two plateau tension values in ACA-added samples and a time-dependent tension minimum in the HOW-only sample. Regarding the observed behavior in ACA-added samples at pH 10, we note three important considerations: (1) even though area was held

(79) Moran, K.; Czarnecki, J. *Colloids Surf., A* **2007**, *292*, 87–98.

(80) Fossen, M.; Kallevik, H.; Knudsen, K. D.; Sjöblom, J. *Energy Fuels* **2007**, *21*, 1030–1037.

(81) Fossen, M.; Sjöblom, J.; Kallevik, H.; Jakobsson, J. *J. Dispersion Sci. Technol.* **2007**, *28*, 193–197.

(82) Hemmingsen, P. V.; Kim, S.; Pettersen, H. E.; Rodgers, R. P.; Sjöblom, J.; Marshall, A. G. *Energy Fuels* **2006**, *20*, 1980–1987.

(84) Sheu, E. Y.; De Tar, M. M.; Storm, D. A. *Fuel* **1992**, *71*, 1277–1281.

(83) Poteau, S.; Argillier, J. F.; Langevin, D.; Pincet, F.; Perez, E. *Energy Fuels* **2005**, *19*, 1337.

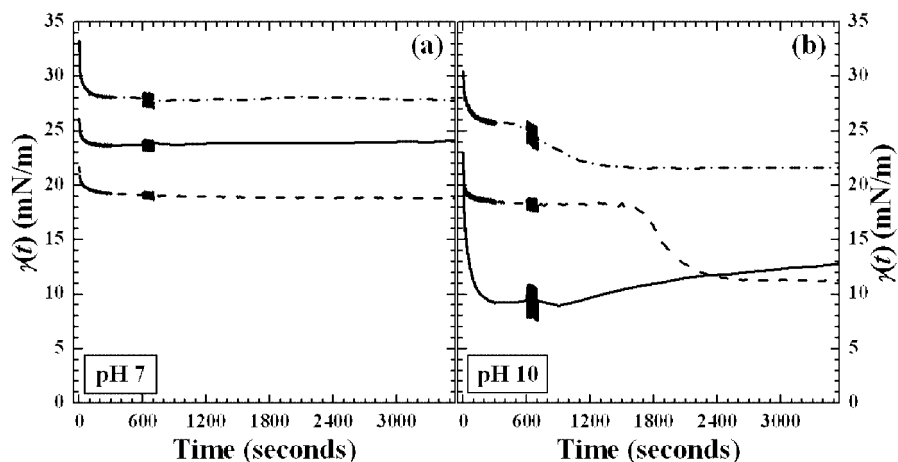


Figure 11. Dynamic interfacial tension during the first hour after formation of a rising model oil drop in 1 wt % NaCl solution at (a) pH 7 and (b) pH 10. Three model oil solutions were tested, all prepared in toluene, including 2 mM 9-ACA (dash-dotted lines), 1 wt % HOW asphaltenes (solid lines), and a mixture of 1 wt % HOW and 5 mM 9-ACA (dashed lines). The apparent bands between 600 and 700 s are actually applied area oscillations, which result in tension oscillations.

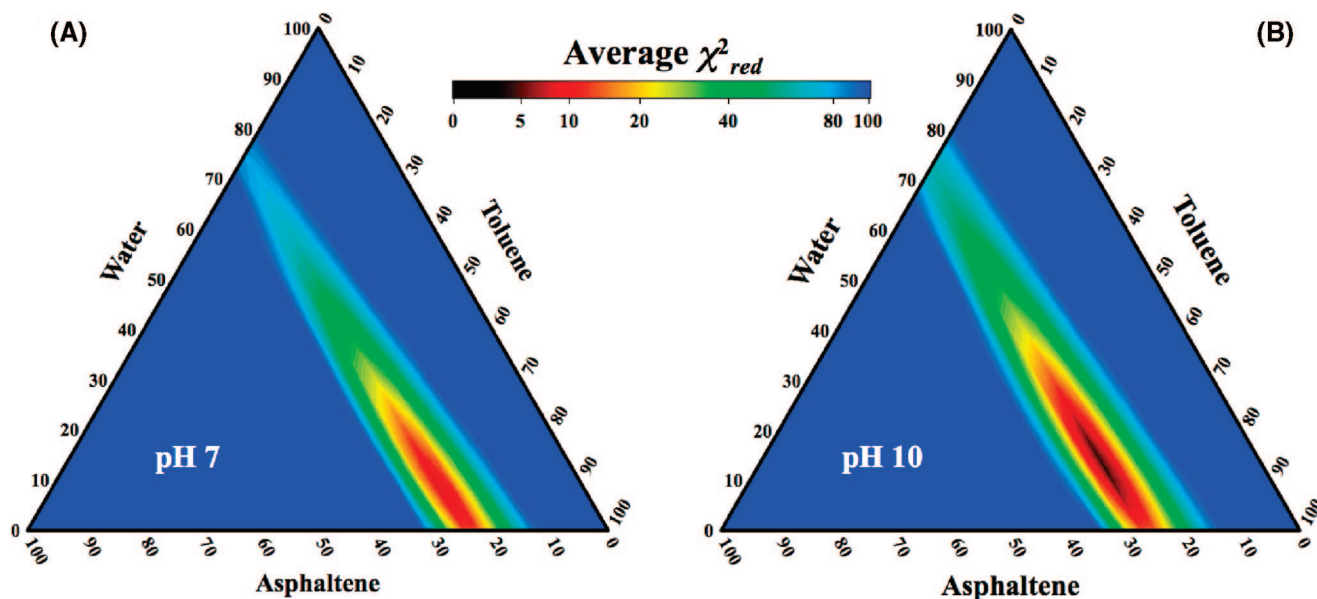


Figure 12. Average χ_{red}^2 as a function of interfacial film composition for emulsions made with 1:1 (v/v) 3 wt % HOW in toluene solution and 1 wt % NaCl in water solution at (a) pH 7 and (b) pH 10. Averages are calculated from six isotopically unique, yet chemically identical, emulsion samples. A total of 861 composition conditions are used to prepare each plot. Other emulsions properties such as R_{avg} , p , and Δ_{film} were fixed at their corresponding values from the optimized fit (Table 8).

constant, the measured drop volume during this initial hour of aging was also constant, (2) the plateau transition was not caused by oscillations, since for some samples with lower ACA concentrations, and no salt in the water, we observed the transition before the first oscillation (not shown), and (3) the observed double-plateau behavior was reproduced several times at pH 10 for samples with varying ACA concentration.

The time-dependent tension minimum at pH 10 should indicate removal of material from the interface, which for the asphaltene-only sample was initially surprising since asphaltenes are often considered irreversibly adsorbed to the interface.^{30,73,74} However, for our system, this may be attributed to the transport of a highly charged acidic asphaltene subfraction into the water phase, similar to what has been documented and modeled for systems containing acidic crudes.^{82,85,86} The unique behavior for samples with ACA

could signify the following two-step process occurs at pH 10: (i) initial rapid adsorption of uncharged species, evident from nearly identical tension values for pH 7 and the first plateau at pH 10 for both samples containing ACA, followed by (ii) deprotonation and subsequent rearrangement of highly surface-active ACA and acidic asphaltene species. This is consistent with our previous inference that at pH 10 the ACA must reside primarily at the interface to maintain its surface activity, while at pH 7 it is free to reside throughout the film.

In Figure 12, we present the variation in average χ_{red}^2 with overall film composition, which provides an effective map of the model fitting optimization. A total of 861 ternary composition inputs ($\phi_{X, film}$ in 2.5% increments) were used to prepare each ternary contour plot. Aside from composition, no other parameters were varied; instead, they were fixed to the values in Table 8.

(85) Filippov, L. K.; Filippova, N. L. *J. Colloid Interface Sci.* **1997**, *187*, 352–362.

(86) Chiwetelu, C. I.; Homof, V.; Neale, G. H. *Chem. Eng. Sci.* **1990**, *45*, 627–638.

The large errors associated with a purely asphaltenic film composition (lower left corner) clearly indicate the film is not entirely composed of asphaltene. As expected, this is also true for films composed entirely of water or toluene. Furthermore, only a narrow area of each plot produced an average χ^2_{red} below 20, which visually occurs at the transition from orange to yellow. Within this section of each diagram, the minimum average χ^2_{red} is sharp with respect to varying asphaltene composition, but less so for varying water and toluene composition. This behavior is related to the contrast conditions used in the experiments, particularly with respect to the limitations on the degree of hydrogenated water or solvent that we could implement before multiple-scattering detracted from the data quality. This is discussed further in the Supporting Information.

Comments on the Applicability of the Core/Shell Model. The core/shell model used here is a first-order approximation of the interfacial structure in that it assumes the volume fraction profile throughout the shell or film is uniform. As such, this uniformity constraint limits our ability to address questions that arise about intralayer contrast among film constituents. However, while it is more realistic to assume a decaying profile of the asphaltenes radially outward from the droplet surface, our modeling attempts with an exponential decay in $\phi_{\text{Asph, film}}$, or even a uniform layer followed by an exponential decay, introduced too many unknown parameters that led to multiple possible profiles, not one unique solution. Again, alleviating the ambiguity that arises from expanding the complexity of the interfacial description requires further careful contrast variation to ensure that such a model can reproduce the scattering for all of the contrast conditions, and does so with a realistic unique solution to the volume fraction profile. We expect the next breakthrough in SANS of asphaltenic emulsions will be the extraction of this emulsion film profile from the data. However, for now, we must accept the shortcomings that accompany the model used here. For example, in the previous discussion, possible changes in the film structure with pH variation and ACA addition were inferred from the changes in the film composition recovered from core/shell modeling. However, these inferences were supported by the interfacial tensiometry observations, which should help to assuage some criticism of this simplified interfacial description.

Conclusions

In the first investigation, we demonstrated the application of small-angle neutron scattering to characterizing water-in-oil emulsions stabilized solely by asphaltene solutions, with a specific focus on the film thickness and its asphaltene composition as a function of three unique host solvents. By focusing on contrast-matched samples, we have evaluated the film thickness and the volume fraction of asphaltene in the films. When compared with emulsion stability, we observed an increasing asphaltene composition (11–30% by volume) in the film that corresponded well with both increasing stability to centrifugal coalescence and increasing film elasticity in dilatational rheology. The average film thickness values were between 100 and 110 Å and otherwise equivalent within error among the three solvents used here. This suggested that, for these Hondo asphaltenes, the asphaltenic makeup of the film, rather than its thickness, largely dictated emulsion stability. We believe this type of interfacial description is invaluable in understanding the mechanisms of emulsion

stabilization in the petroleum industry, and its scarcity in the petroleum literature signifies its novelty.

In the second investigation, we measured several properties of asphaltenically stabilized water-in-model oil emulsions, including total droplet surface area per sample volume (S/V) and the thickness of the stabilizing interfacial film (Δ_{film}). Using a modified polydisperse core/shell form factor and isotopic ($^1\text{H}/^2\text{H}$) contrast variation, we were able to ascertain the entire film composition. It is our understanding that this is the first such *in situ* evaluation of the total composition for asphaltenic interfacial films in water-in-model oil emulsion samples, as opposed to spread mono- or multilayers and extruded thin films. Interestingly, our investigation reveals that while HOW asphaltenic interfacial films are primarily composed of solvent and asphaltene, water has a measurable presence in these films. Our analyses indicate an increase in film water composition with increasing pH and 9-ACA addition, which together suggest that the polar moieties of asphaltenes, in this case carboxylic acids, dictate the overall interfacial film structure.

Our current application of SANS has enabled evaluation of real emulsion droplet interfaces, and we anticipate its use in future endeavors to not only offer insight on stabilization mechanisms but also answer questions regarding the mechanisms of *destabilization* of emulsions as they pertain to changes in the interfacial film thickness and composition under a variety of mechanical, thermal, electrical, magnetic, or chemical stresses. Furthermore, the presence of water within asphaltenic films leads to many scientific questions for future work, including the impact of film water composition in emulsion stability, how this composition may change in the presence of chemical demulsifiers, and the nature of water transport to/from/within the film.

Acknowledgment. We are grateful to the Kilpatrick Joint Industrial Consortium for their financial support, particularly Shell, ExxonMobil, ConocoPhillips, NALCO, Champion Technologies, and PetroBeam. This work utilized facilities supported in part by the National Science Foundation under Agreement No. DMR-0454672. We acknowledge the support of the National Institute of Standards and Technology, U.S. Department of Commerce, in providing the neutron research facilities used in this work. In particular, we would like to thank Boualem Hammouda, Steve Kline, Paul Butler, John Barker, and David Mildner. Results shown in this report are derived from work performed at Argonne National Laboratory. Argonne is operated by UChicago Argonne, LLC, for the U.S. Department of Energy under contract DE-AC02-06CH11357. We are particularly grateful for the help of Pappanan Thiyagarajan, Denis Wozniak, Jyotsana Lai, and Ed Lang of the Intense Pulsed Neutron Source at Argonne. We thank Salomon Turgman and Matthew Smith for their assistance in sample preparation and instrument operation during the experiments. Finally, we appreciate the rapid sample by Wayne Moffat and the Analytical Chemistry laboratory at the University of Alberta.

Supporting Information Available: Details on (1) the SLDs of the materials, (2) the emulsion rinsing procedure, (3) the protocol for microscopic determination of the droplet size distribution, (4) the erroneous determination of droplet size using only S/V obtained from SANS, (5) simultaneous core/shell fits and corresponding χ^2_{red} values, and (6) the sensitivity of the χ^2_{red} value on film composition. This material is available free of charge via the Internet at <http://pubs.acs.org>.

LA802095M